AGU PUBLICATIONS

Paleoceanography

RESEARCH ARTICLE
10.1002/2015PA002792

Key Points:
- Upwelling intensity and regional-global climatic and oceanographic changes affect primary productivity
- Diatom input governs the benthic foraminiferal faunal composition
- Benthic foraminiferal fauna indicates low oxygen conditions of varying severity

Correspondence to:
C. L. McKay,
Claire.McKay@geol.lu.se

Citation:
McKay, C. L., H. L. Filipsson, O. E. Romero, J.-B. W. Stuut, and S. Björck (2016), The interplay between the surface and bottom water environment within the Benguela Upwelling System over the last 70 ka, *Paleoceanography*, *31*, 266–285, doi:10.1002/2015PA002792.

Received 16 FEB 2015
Accepted 7 JAN 2016
Accepted article online 13 JAN 2016
Published online 20 FEB 2016

The interplay between the surface and bottom water environment within the Benguela Upwelling System over the last 70 ka

C. L. McKay[1], H. L. Filipsson[1], O. E. Romero[2], J.-B. W. Stuut[2,3], and S. Björck[1]

[1]Department of Geology, Lund University, Lund, Sweden, [2]MARUM–Center for Marine Environmental Sciences, Universität Bremen, Bremen, Germany, [3]Marine Geology Department, NIOZ-Royal Netherlands Institute for Sea Research, Den Burg, Netherlands

Abstract The Benguela Upwelling System (BUS), located between 30 and 20°S, is one of the fundamental high-productivity systems of the world ocean. The BUS has previously been studied in terms of primary productivity and ecology over glacial-interglacial timescales; however, the response and coupling with the benthic environment have received little attention. Here, for the first time, we present a high-resolution reconstruction of the BUS highlighting the link between surface and benthic productivity and their response to climatic and oceanographic changes over the last 70 ka. The study is based on benthic foraminiferal faunal analysis together with analyses of diatom assemblages, grain size of the terrigenous fraction, and stable O and C isotopic and bulk biogenic components of core GeoB3606-1. We reveal significant shifts in benthic foraminiferal assemblage composition. Tight coupling existed between the surface and bottom water environment especially throughout marine isotope stages 4 and 3 (MIS4 and MIS3). Due to the high export production, the site has essentially experienced continuous low oxygen conditions; however, there are time periods where the hypoxic conditions were even more notable. Two of these severe hypoxic periods were during parts of MIS4 and MIS3 where we find an inverse relationship between diatom and benthic foraminifera accumulation, meaning that during times of extremely high phytodetritus export we note strongly suppressed benthic productivity. We also stress the importance of food source for the benthos throughout the record. Shifts in export productivity are attributed not only to upwelling intensity and filament front position, but also, regional-global climatic and oceanographic changes had significant impact on the BUS dynamics.

1. Introduction

The Benguela Upwelling System (BUS) is one of the major eastern boundary upwelling systems and is one of the most productive regions of the world ocean. While long-term trends in the BUS are well documented, in particular the influence of the Southern Ocean from the Pliocene (5.3 Ma) to the Quaternary [*Lange et al*., 1999; *Ufkes et al*., 2000; *Berger and Wefer*, 2002a; *Heinrich et al*., 2011], few studies exist for relative short-term benthic ecological changes in the order of thousands of years. While the BUS has been studied frequently in terms of primary productivity, trophic levels, and ecology [*Romero et al*., 2003; *Romero*, 2010; *Lamont et al*., 2014; *Schukat et al*., 2014; *Romero et al*., 2015], only a few studies have examined the coupling between surface primary productivity and the benthic environmental response [e.g., *Brüchert et al*., 2000]. Furthermore, the existing research on pelagic-benthic coupling has either considered the modern BUS in terms of organic flux causing low oxygenation at the seafloor or has covered longer timescales than the Quaternary and at lower resolution [*Bailey*, 1991; *Brüchert et al*., 2000].

Upwelling intensification in the BUS has been attributed to changes in the strength and zonality of the trade wind system [*Berger and Wefer*, 2002b; *Little et al*., 1997; *Stuut et al*., 2002; *Summerhayes et al*., 1995; *Sydeman et al*., 2014]. Factors that determine the productivity dynamics in the BUS are well reported, such as upwelling source, seaward extension of the chlorophyll filaments, and shelf waves [*Berger and Wefer*, 2002b; *Müller et al*., 2013]. Of further note is that fluctuations in diatom productivity at glacial-interglacial timescales in the BUS are not synchronous with upwelling intensity during the late Quaternary [*Diester-Haass*, 1985]. This "Walvis Opal Paradox" [*Berger and Wefer*, 1996] juxtaposes evidence for low opal accumulation during glacial periods within the Quaternary [*Oberhänsli*, 1991]. The paradox applies to the BUS where diatom production has been found to exhibit a low level of response to climate fluctuations [*Anderson et al*., 2001]. However,

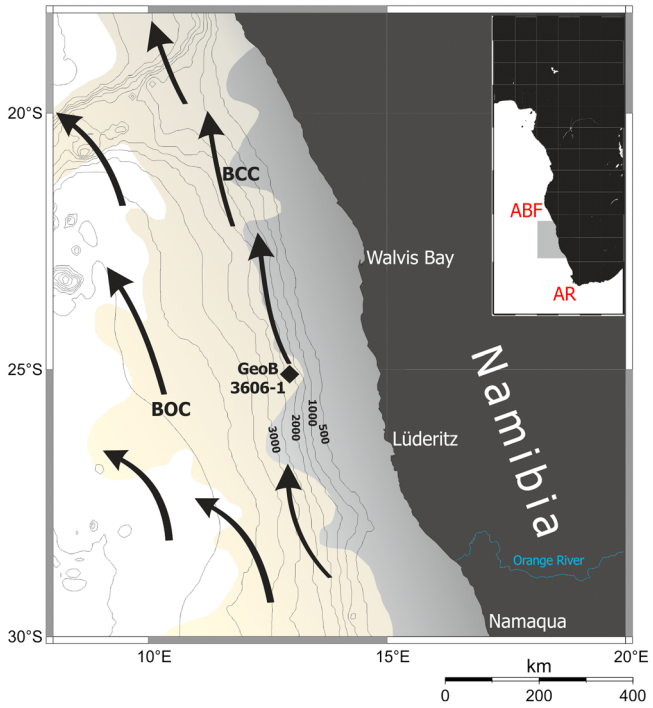

Figure 1. Location of site GeoB3606 (black diamond). Black arrows represent surface water circulation in the BUS [after *Shannon*, 1985; *Lutjeharms and Stockton*, 1987]. Darker shading indicates the present area of strong coastal upwelling, and light shading represents the modern extensions of the upwelling filaments. BCC: Benguela Coastal Current. BOC: Benguela Oceanic Current. Inset is the locality of the BUS off the coast of Namibia in the SE Atlantic Ocean, the ABF: Angola-Benguela Front and the AR: Agulhas Retroflection.

paleoreconstructions of how the seafloor environment responded to these shifts in the dynamics of the BUS are scarce. The fundamental question for understanding variable short-term productivity and potential benthic community shifts relates to the combined effects of oceanographic and atmospheric changes at millennial timescales.

Thus, it is vital to recognize the gap in our knowledge by analyzing benthic foraminiferal responses to changes in primary productivity at higher temporal resolution in order to evaluate the dynamics of the BUS and the reaction of the benthos during rapid climate changes over millennial timescales. Our study is novel as we assess the relationship between the surface productivity and the consequences for the benthic environment by focusing on benthic foraminiferal community composition at millennial timescales within the late Quaternary. By considering the fact that modern primary productivity is concentrated at the upwelling filament front [*Lutjeharms and Stockton*, 1987], we hypothesize that past variations in its position and surface productivity will impact upon the bottom water environment. Our approach consists of new high-resolution analyses of benthic foraminiferal faunal assemblages, planktonic and benthic foraminiferal stable oxygen and carbon isotope measurements, grain size analysis, and end-member modeling of the terrigenous fraction, in tandem with previously published diatom accumulation and bulk biogenic data [*Romero et al.*, 2003; *Romero*, 2010; *Romero et al.*, 2015], to describe the variations in paleoproductivity, the bottom water environment, and also regional climate conditions and dynamics over the last 70 ka at site GeoB3606, 25°S off Namibia, SW Africa.

2. Study Site

Our study focuses on the coupling between pelagic and benthic ecosystems and how this relationship has varied over time in relation to large-scale atmospheric and climate shifts. To do this, we utilize a multiproxy approach by analyzing the marine sediment core GeoB3606-1 recovered at 25°S within the central BUS (Figure 1).

2.1. Atmospheric and Oceanographic Characteristics

The major area of the BUS is located at 20–30°S adjacent to the SW African coast. The BUS is unique as it is bordered by warm water regimes: the Angola-Benguela Front to the north and the Agulhas Retroflection to the south (Figure 1).

The present-day Benguela area has a wind field dominated by the prevailing SE trade wind system, which drives the upwelling of cold, nutrient-rich water of the Benguela Current (BC) from depths of 200–300 m to the sea surface [*Shannon*, 1985]. The strongest and more continuous upwelling occurs near Lüderitz, Namibia, at 26–27°S [*Lutjeharms and Meeuwis*, 1987]. North of this latitude, upwelling favorable winds are perennial, whereas in the southern BUS, stronger seasonality occurs with distinct upwelling maxima during

spring and summer [*Shannon and Nelson*, 1996; *Romero et al*., 2003]. Upwelling occurs close to the coast on the inner shelf [*Wefer et al*., 1998] in a number of distinct cells and filaments in a continuous belt along the coastline. These cells form at the maximum wind stress curl and also where coastline orientation changes [*Lutjeharms and Meeuwis*, 1987]. At the shelf break, a thermal front defines the boundary of the seaward extent of upwelled waters. Frequently disturbed by small filaments and eddies, this highly convoluted front can extend up to 750 km offshore [*Lutjeharms and Meeuwis*, 1987] affecting the dynamics and spatial variability of primary production and the transport of nutrients and microorganisms [*Shillington*, 1998].

Different water masses enter the BUS, namely, South Atlantic Central Water (SACW) with waters of sub-Antarctic origin and also the Indian Ocean via the Agulhas Current being important constituents. These subsurface waters are underlain by Antarctic Intermediate Water (AAIW) at 300–800 m, Upper Circumpolar Deep Water (UCDW) at 800–1200 m, and North Atlantic Deep Water (NADW) at 1200–2500 m depth [*Shannon*, 1985]. AAIW is an important carrier of nutrients from the Southern Ocean [*Sarmiento et al*., 2004] as it transmits the high silicate content signal into the silicate-poorer, low-latitude waters [*McCartney*, 1977]. At present our core site at 1785 m is bathed in NADW.

Several major changes in current and front systems may potentially influence the hydrography and productivity dynamics of site GeoB3606, such as the increased flow of warm surface waters of the Agulhas Current [*Duncombe Rae et al*., 1992]. Over time, the changes in hydrography and strength of the trade winds are coupled to climatic shifts and also impact the nutrient levels of the surface waters and according also production. Furthermore, as a result of the latitudinal length of the BUS, seasonality of winds and the orientation of the coastline differ between upwelling cells [*Lutjeharms and Meeuwis*, 1987] and hence may cause spatial variations in the surface productivity and biomass signals within the whole upwelling system. Furthermore, the stability of these spatial variations changes through time due to changes in the strength of the southeasterly trade winds and their latitudinal migration, displacement of the upwelling front and filament locality, rapid sea level variations, and the source of the upwelled waters [*Romero et al*., 2015].

2.2. Primary Productivity and Oxygen Levels

As eastern boundary upwelling systems are so highly productive, the bottom water environment is often susceptible to low oxygen conditions due to oxygen consumption as a result of degradation of sinking phytodetritus [*Levin et al*., 2009]. The BUS is no exception, and its low oxygen water variability is governed by varying scales of remote and local forcing such as upwelling intensity and resulting production [*Monteiro and Van der Plas*, 2006]. Furthermore, the BUS is also characterized by poleward transport of low oxygenated water along the entire coast of Africa [*Müller et al*., 2013]. This low oxygenated water promotes extensive seafloor hypoxia (0.5–1 mL O_2 L^{-1}) and anoxia ($<$0.5 mL O_2 L^{-1}) and the formation of sulphidic sediments [*Bailey*, 1991]. Overall, the implications for biota and fish stocks have been well documented over the years [*Copenhagen*, 1953; *Pieterse and van der Post*, 1967; *Shannon and Jarre-Teichemann*, 1999]; however, little has been reported regarding the benthic meiofauna community.

3. Methodology

3.1. Core Location and Sampling Strategy

Our study focuses on gravity core GeoB3606-1, retrieved 175 km off the modern Namibian coastline, southwest Africa on the upper continental slope at 1785 m water depth (Figure 1) during R/V *METEOR* cruise M34/1 (25°28′S, 13°05′E) [*Bleil and Cruise Participants*, 1996]. The 1074 cm long, 13 cm in diameter sediment core consists of nannofossil-bearing siliceous clays [*Bleil and Cruise Participants*, 1996]. No signs of turbidites were evident in the core, so we have no reason to doubt a continuous stratigraphy throughout the entire record. For our study, sediment samples (10 cm^3) were taken at 5 cm intervals enabling microfossil, geochemical, and stable O and C isotopic and grain size analyses to be utilized at an average sample interval ranging between 100 and 250 years. Archived core material is stored at MARUM–Center for Marine Environmental Sciences (MARUM) (Bremen University, Germany).

3.2. Chronology

The chronology of gravity core GeoB3606-1 is constrained by nine accelerator mass spectrometric (AMS) ^{14}C age determinations: six previously published in *Romero et al*. [2003] and *Romero* [2010] and three newly determined dates measured on the planktonic foraminifera *Globigerina bulloides* and *Globigerina inflata* ($>$150 μm fraction) at

Table 1. Acceleration Mass Spectrometer ^{14}C Dates and Calibrated Calendar Dates (ka) of Gravity Core GeoB3606-1

Leibniz/Lund Laboratory Identification No.	Depth (cm)	AMS ^{14}C Age (year B.P.)	Analytical Error ($\pm1\sigma$) (yrs)	Error $\pm2\sigma$ (years)	Age (ka B.P.)	Analyzed Material	Reference
LuS 10720	38	6,210	90	90	6,533	*G. bulloides*	This study
KIA17057	73	9,895	45	80	10,660	*G. bulloides* and *N. pacyderma*	*Romero et al.* [2003]
KIA17055	98	10,895	50	90	12,150	*G. bulloides*	*Romero et al.* [2003]
KIA17054	148	13,280	60	90	14,935	*G. bulloides*	*Romero et al.* [2003]
LuS10721	173	13,580	100	100	15,790	*G. bulloides*	This study
KIA17053	198	16,990	90	85	19,805	*G. bulloides*	*Romero et al.* [2003]
LuS10722	403	31,250	300	85	34,489	*G. bulloides* and *G. inflata*	This study
KIA16992	628	40,230	1,480	80	44,998	Mixed planktonics	*Romero et al.* [2003]
KIA16991	703	42,770	2,120	70	48,907	Mixed planktonics	*Romero et al.* [2003]

the Radiocarbon Laboratory at Lund University, Sweden (Table 1). Where an insufficient amount of pristine tests were present, mixed planktonic specimens were dated. The radiocarbon ages of all nine samples were converted into calendar years, and a new age model was created using the OXCAL 4.2 program with the marine calibration curve MARINE13 [*Reimer et al.*, 2013]. A reservoir age of 400 years was employed as the mean value for the South Atlantic Ocean at 20°S latitude [*Bard*, 1988; *Mollenhauer et al.*, 2003] which has been utilized in previous studies in the BUS [*Dewar et al.*, 2012]. However, we acknowledge that reservoir ages in this region may vary through time in response to variable rates of upwelling and upwelling of older subsurface waters in the BUS [*Mollenhauer et al.*, 2003]. All ages are reported in calendar years before present (B.P.), where present is 1950 and in unit thousand years (ka).

3.3. Benthic Foraminiferal Faunal Analyses

For benthic foraminiferal faunal analyses, 10 cm^3 of sediment was sampled, freeze dried, wet sieved over 63–125 μm, 125–250 μm, 250–500 μm, and >500 μm sieves, and oven dried at 40°C. Faunal analyses of 300 specimens were determined to the species level using each of the three >125 μm fractions separately. From these three individual fractions, the total specimen counts were totaled for each depth. Analyses were undertaken at approximately 10 cm resolution (corresponding to 660 year resolution on average) and higher resolution where surface productivity exhibits rapid fluctuations. Counts were adjusted accordingly for split samples, and taxonomic identification follows *Loeblich and Tappan* [1987], *Jones* [1994], and the World Register of Marine Species [*WoRMS Editorial Board*, 2015] database. The general faunal characteristics are expressed as Shannon diversity and dominance (percentage of most frequent species). Taxa that display an average relative abundance of >5% were selected for statistical analyses. To account for the changing sedimentation rate, benthic foraminifera accumulation rates (BFARs) were calculated as follows: BFAR (number of specimens $cm^{-2}\,ka^{-1}$) = BF × SAR where BF is the number of benthic foraminifera specimens per cm^3 of sediment and SAR is the sediment accumulation rate ($cm\,ka^{-1}$).

The relative abundance data of benthic foraminifera were analyzed by CABFAC factor analysis which is a refinement of principal component analysis as it rotates the factors orthogonally [*Murray*, 1991]. Only key species (those that accounted for >5% of the population in at least one sample) were used for factor analysis which was performed using PAST software [*Hammer et al.*, 2001].

3.4. Stable O and C Isotopic Analysis

From the benthic foraminiferal faunal analyses, specimens of the following benthic foraminifera species were picked from the 250–500 μm fraction to achieve an analytical weight of 0.02 mg for each species sampled at 5 cm intervals when in sufficient abundance: epifaunal *Cibicides wuellerstorfi*, deep infaunal *Globobulimina turgida*, and epifaunal-shallow infaunal *Oridisalis unbonatus*. All tests were cleaned ultrasonically for 5 s, suspended in methanol, and subsequently dried at 50°C. The cleaned samples were contained in individual reaction vials for each sample depth and reacted with 3 drops of H_3PO_4 within the Kiel device preparation line. Stable carbon and oxygen isotopic analysis was measured by a Finnigan MAT 253 mass spectrometer at the Bjerknes Centre for Climate Research, University of Bergen, Norway. By convention, isotope ratios are reported relative to the Vienna Peedee belemnite (VPDB). The foraminiferal isotopic values are reported in δ notation relative to the VPDB scale with a precision of over 0.08‰ for $\delta^{18}O$ and 0.03‰ for $\delta^{13}C$, respectively.

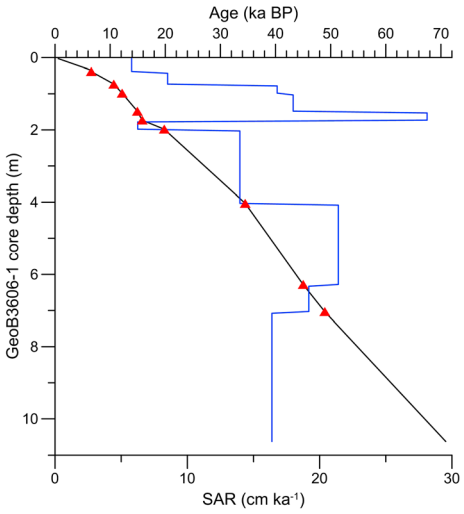

Figure 2. Age model (black line) obtained from nine calibrated ^{14}C dates and sediment accumulation rates (cm ka^{-1}; blue line) from 70 ka to present for upper 1063 cm of core GeoB3606-1. Red triangles denote ^{14}C dates. Absolute values are summarized in Table 1.

Previously, planktonic foraminifera species *Globigerina bulloides* and *Globorotalia inflata* from the 250–500 μm fraction were measured for stable oxygen and carbon isotopic analysis using the same method at MARUM, Bremen University, Germany [*Romero et al.*, 2003]. Precision was over 0.08‰ for δ^{18}O and 0.04‰ for δ^{13}C, respectively, and the δ^{13}C data were previously unpublished.

3.5. Grain Size Analysis and End-Member Modeling

Terrigenous sediments deposited on the seafloor are a mixture of a pelagic component carried by wind and a hemipelagic component transported by rivers to the shelf and later transported and reworked by alongshore currents. The flux of hemipelagic sediments (fine and fluvial muds) associated with continental runoff can thus be used as a proxy for continental humidity since an increase of fluvial sediments in the marine sediment record implies stronger river discharge to the sea [*Prins and Weltje*, 1999]. Aeolian sediments being coarser grained are distinguishable from the fluvial fraction allowing estimation of aridity and also intensity of the transporting winds through grain size measurements of the dust fraction [*Sarnthein et al.*, 1981]. Therefore, to determine the origin and quantity of the terrigenous fraction, grain size analysis and subsequently end-member modeling was utilized.

At 5 cm intervals, 0.5 g of sediment was subsampled, corresponding to a time resolution of 330 years on average, and the biogenic compounds were removed from the sediment. Organic carbon was removed by heating the sample to 100°C in H_2O_2 (35%). Subsequently, the samples were treated for 1 min with HCl (10%) at 100°C to remove $CaCO_3$ and biogenic opal was removed with NaOH. Measurements were performed in demineralized and degassed water in order to improve the signal-to-noise ratio of the particle-size analysis. Grain size distributions were measured using a Beckman Coulter laser particle sizer LS200, resulting in 92 size classes ranging from 0.4 to 2000 μm. All pretreatments and the grain size measurements were completed at MARUM (Bremen). Numerical end-member modeling was employed to differentiate between distinctive sediment subpopulations within the grain size distribution. The algorithm EMMA was used [*Weltje*, 1997] and the end-members chosen based on the goodness of fit statistics by calculating the coefficient of determination (r^2) which represents the quantity of variance of each grain size class that can be replicated by the approximated data. The outcome of the model represents real particle-size distributions whose end-members are a statistically unique solution. Further details are provided in *Weltje and Prins* [2003].

3.6. Diatom Analysis

Diatom analysis was undertaken at 5 cm resolution and previously published by *Romero et al.* [2003], *Romero* [2010], and *Romero et al.* [2015]. To account for the changing sedimentation rates, diatom accumulation rates (DARs) were calculated as follows: DAR (number of valves cm^{-2} ka^{-1}) = $D \times$ SAR where D is the number of diatom valves per cm^3 of sediment and SAR is the sediment accumulation rate (cm ka^{-1}).

3.7. Bulk Geochemical Analysis

Bulk geochemical analyses were undertaken at 5 cm intervals with an analytical precision of 0.5%, and the detailed methods and results are published in *Romero et al.* [2003] and *Romero* [2010].

4. Results

4.1. Age Model

The age model of core GeoB3606-1 is based on nine radiocarbon dates on planktonic foraminifera (Table 1 and Figure 2). The record extends back to 70 ka through linear interpolation. The resulting sedimentation rates range between ~5.8 and 28.1 cm ka^{-1} (average of approximately 16.7 cm ka^{-1}) reaching highest values after 15 ka.

Table 2. Summary of Benthic Foraminiferal Species Ecology

Factor	Variance (%) Total Variance	Dominant Species	Score
1	66.25	*E. exilis*	4.6158
2	17.87	*B. aculeata*	−4.4992
3	7.13	*E. exigua*	−1.704
		N. iridea	1.0529
		N. turgida	−1.8358
		O. umbonatus	−1.1746
4	2.83	*C. laevigata*	4.1209
		N. iridea	−2.7892

Our benthic isotope data (see subsequent section 4.3) confirm the age model; for example, the timing of the Last Glacial Maximum (LGM) in particular is distinct by the increase in *C. wuellerstorfi*-derived $\delta^{18}O$ values from 26 to 19 ka, which is consistent with the timing of the global LGM [*Clark et al.*, 2009]. In addition, we also follow the established definition of *Lisiecki and Raymo* [2005] for the boundaries of the marine isotope stages (MIS), which are defined as follows: termination of MIS4 is defined at 59 ka, and MIS3 occurs at 59–30 ka, MIS2 at 30–14 ka, and MIS1 at 14–0 ka.

4.2. Benthic Foraminiferal Faunal Assemblages

Our interpretation of the benthic foraminiferal fauna is based on their ecological preferences (Table 2). Site GeoB3606 documents both rapid and long-term changes in benthic productivity and the causal environmental conditions during the last 70 ka. The benthic foraminiferal fauna is characterized by a diverse calcareous assemblage consisting of 57 species, dominated by *Eubuliminella exilis*. The most prominent species are displayed in Figure 3. Several benthic foraminiferal species persist throughout the entire record including *Bulimina aculeata*, *Cassidulina laevigata*, and *Oridisalis umbonatus* but in varying abundance. The benthic foraminiferal diversity of core GeoB3606-1 ranges from Shannon diversity *H*(*S*) values of 0.29–2.84 and exhibits short-term fluctuations throughout the core with the lowest diversity occurring during MIS3 and highest during MIS1 where it is relatively stable (Figure 3). The factor analysis resulted in four factors explaining 94% of variance consisting of eight significant species (Figure 3 and Table 3). The factor analysis exhibits several shifts in the dominant factor which enabled us to identify a total of six different benthic foraminiferal phases (denoted assemblage A to F in Figure 3 and Table 4) within the GeoB3606-1 record. The first, assemblage A, occurs within late MIS4, an

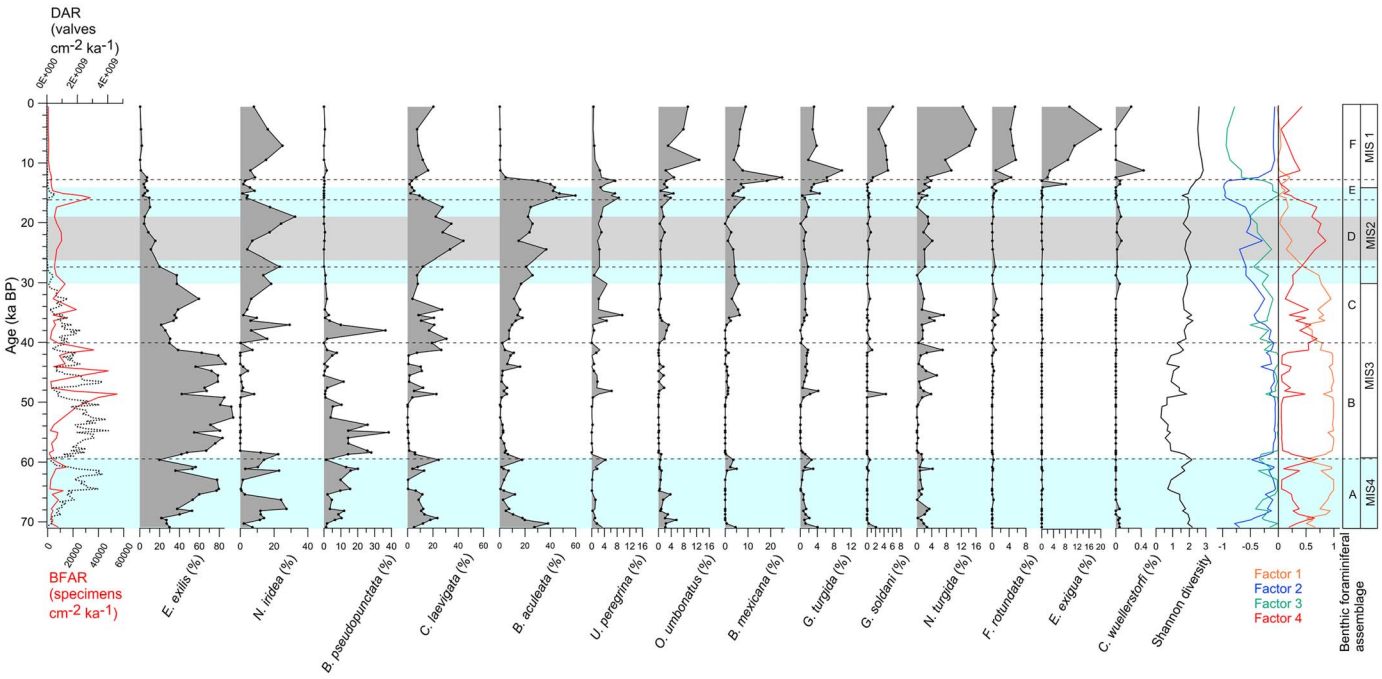

Figure 3. GeoB3606-1 downcore changes in diatom accumulation rate (valves cm^{-2} ka^{-1}), benthic foraminiferal accumulation rate (specimens cm^{-2} ka^{-1}), relative abundance (%) of the most common benthic foraminifera species Shannon diversity index, and factor analysis loadings. Shadings are as follows: late MIS4: 70–59 ka, MIS2: 30–14 ka, and LGM: 26–19 ka. Benthic foraminiferal assemblages are labeled A–F, and dotted lines represent their boundaries according to the factor analysis. Note the different size *x* axes of the benthic foraminiferal abundance data to emphasize the more abundant taxa.

Table 3. Benthic Foraminiferal Assemblages Revealed by Factor Analysis

Benthic Foraminifera Species	Benthic Ecological Significance	Reference
Bolivina pseudopunctata	Indicates low oxygen conditions and fresh phytodetritus input, opportunistic species	*Pérez et al.* [2001]
Bulimina aculeata	Can tolerate short-term low oxygen conditions	*Nardelli et al.* [2014]
Cassidulina laevigata	High organic input	*Corliss and Emerson* [1990]
Cibicides wuellerstorfi	Well-oxygenated bottom water conditions	*Mackensen et al.* [1995]
Epistominella exigua	Opportunistic species	*Schmiedl and Mackensen* [1997]
Eubuliminella exilis	Can tolerate persistent low oxygen conditions and fresh phytodetritus input	*Caralp* [1989]
Globobulimina turgida	Low oxygen conditions, degraded organic matter	*Sweetman et al.* [2009]
Nonionella iridea	High phytodetritus input, high productivity	*Polovodova-Asteman et al.* [2013]
Nonionella turgida	Opportunistic species that prefers high food availability and tolerant to reduced oxygen conditions	*Van Der Zwaan and Jorissen* [1991]
Oridisalis umbonatus	Resides in more oxygenated bottom water where a low flux of highly degraded organic matter is sustained	*Mackensen* [1985]

assemblage dominated by *E. exilis* (up to 80%), with *B. aculeata* (up to 40%) and *Nonionella iridea* (maximum 25%) during times of moderate *E. exilis* abundances. The average BFAR of this interval entitled assemblage A is comparatively moderate at 5400 specimens $cm^{-2}\,ka^{-1}$.

Assemblage B occurs in early MIS3 (59–40 ka) where *E. exilis* fluctuates from a minimum of 20% to a maximum of 95% and is accompanied by *Bolivina pseudopunctata* (0–40%) as an important accompanying species. BFAR fluctuates at great range from 860 to 29500 (average = 13730) specimens $cm^{-2}\,ka^{-1}$. A third assemblage (C) within the record is notable during late MIS3 (40 to 30 ka) where *E. exilis* decreases to more moderate levels (34% on average) and *N. iridea* and *C. laevigata* (both up to 30%) become more prominent. BFAR continues to show great fluctuations ranging from 650 to 14450 (average = 8235) specimens $cm^{-2}\,ka^{-1}$.

Table 4. Synthesis of the Palaeoproductivity, Processes and Mechanisms, and Benthic Response at Site GeoB3606

Benthic Foraminiferal Phase	Age (ka)	Climatic Interval	Palaeoceanographic Setting in the SE Atlantic	Primary Productivity Regime	Benthic Response
A	70–59	late MIS4	Intense upwelling, inflow of Si-rich Antarctic waters with additional fluvially derived Si	Extremely high DAR and TOC. Upwelling indicating diatoms	*E. exilis* dominant with *B. aculeata* and *N. iridea* as important secondary species. Low oxygen conditions at the seafloor.
B	59–40	early MIS3	Intense upwelling, inflow of Si-rich Antarctic waters with additional fluvially derived Si	Extremely high DAR and TOC. Upwelling indicating diatoms	*E. exilis* dominant. Low oxygen conditions at the seafloor.
C	40–30	late MIS3	Sea level decrease, upwelling filament migrates offshore	High DAR	*E. exilis* still dominant but *C. laevigata* and *B. aculeata* become more prominent as DAR decreases. Low oxygen conditions at the seafloor.
D	30–16	MIS2	Further sea level decrease, upwelling filament migrates farther offshore	Low DAR, relatively higher $CaCO_3$	*B. aculeata*, *C. laevigata* and *N. iridea* assemblage: relative recovery in the bottom water oxygen levels.
E	16–14	MIS2	Cooler SSTs	Relative increase in DAR	*B. aculeata* dominates the assemblage in response to a peak in DAR which does not hamper the bottom water oxygenation to the extent of MIS4 and MIS3, evidenced from low *E. exilis* abundance.
F	14–0	MIS1	Upwelling intensity decreases. Reactivation of the AMOC, Agulhas leakage. Warmer SSTs.	Decline in DAR and a shift to calcareous producers. Coastal, planktic diatom species.	*E. exigua*, *O. umbonatus* and other benthic foraminiferal species previously of low abundance in the record dominate the assemblage. Slightly improved bottom water oxygenation.

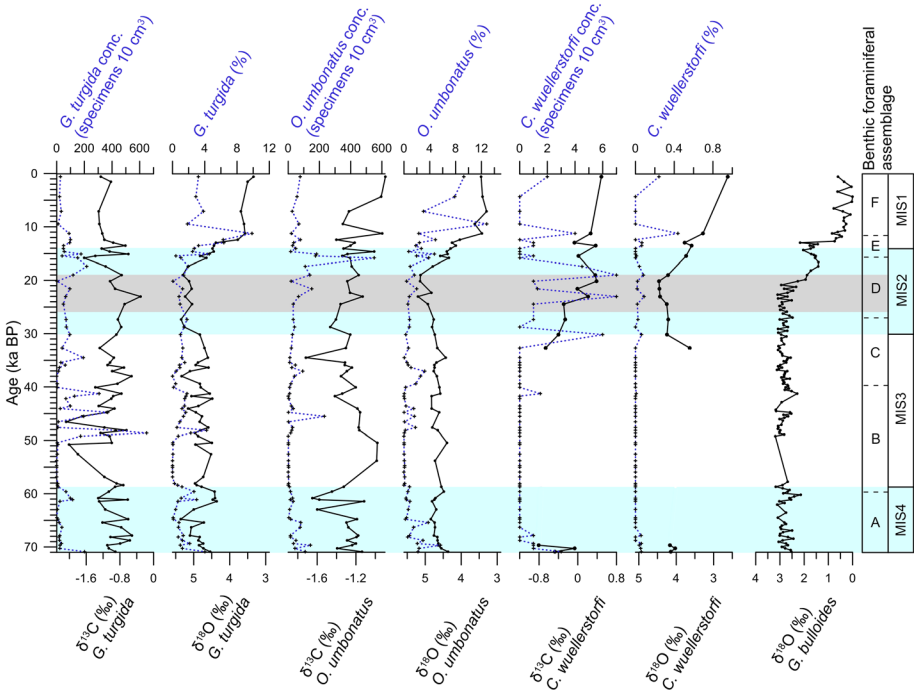

Figure 4. GeoB3606-1 $\delta^{18}O$ and $\delta^{13}C$ for the three benthic foraminiferal species *G. turgida*, *O. umbonatus*, and *C. wuellerstorfi* and planktonic foraminiferal species *G. bulloides* (black lines). Species concentrations and relative abundances are also shown (blue lines). Shadings are as follows: late MIS4: 70–59 ka, MIS2: 30–14 ka, and LGM: 26–19 ka. Benthic foraminiferal assemblages are labeled A–F, and dotted lines represent their boundaries according to the factor analysis.

Within MIS2, at 27.5 ka, the fourth assemblage (assemblage D) is composed mainly of *C. laevigata* and *B. aculeata* (up to 45 and 40%, respectively). The BFAR throughout this interval is at relatively moderate-high levels, averaging at 7650 specimens $cm^{-2}\,ka^{-1}$.

Subsequently, the factor analysis highlights a fifth assemblage (E) from 16 to 12 ka dominated by *B. aculeata* (up to 60%) with a high BFAR of 10940 specimens per $cm^{-2}\,ka^{-1}$ on average. Finally, within MIS1, assemblage F is defined by a shift in composition occurring from 12 ka onward (Figure 3) with the overall highest diversity (Shannon values up to 2.84) consisting of several species which were previously $<4\%$ in abundance such as *Epistominella exigua* (up to 20%) and *Nonionella turgida* (up to 16%). Throughout MIS1, BFAR declines to the lowest values of the entire record (average = 715 specimens $cm^{-2}\,ka^{-1}$) and does not fluctuate at magnitudes of the previous assemblages.

4.3. Stable O and C Isotopic Analysis

The benthic foraminiferal species *G. turgida* and *O. umbonatus* were present throughout the entire core (Figure 4). *Cibicides wuellerstorfi* was rarely present during MIS3 and MIS4. The planktonic species *Globigerina bulloides* was abundant throughout the record except within early MIS3.

During MIS4 moderately high $\delta^{18}O$ values were recorded by *C. wuellerstorfi* (average 4.2‰ based on three measurements) and *G. turgida* (average 5‰). $\delta^{18}O$ values for *O. umbonatus* remains around 4.8‰ and exhibits a slight shift of 0.5‰ on average throughout MIS3. In contrast, *G. turgida* shows an average $\delta^{18}O$ of 4.83‰ with fluctuations ranging from 4.3 to 5.25‰ through MIS3. Similarly, the planktonic isotope signal from *G. bulloides* only fluctuates at low amplitudes around 3.0‰ within MIS3. During MIS2, all benthic $\delta^{18}O$ values show considerably higher values in comparison to the rest of the record, with *C. wuellerstorfi* in particular exhibiting a distinct shift of 0.9‰ toward higher values between 26 and 19 ka. At 19 ka, a notable decrease in $\delta^{18}O$ values of the planktonic *G. bulloides* and *G. inflata* record (decreasing from 3 to 1.5‰ on average) occurs. Subsequently, at 16 ka a slight reverse back to values of approximately 4.45‰ for *G. turgida* and 4.3‰ for *O. umbonatus* follows. During MIS1 a fundamental shift to discernibly lower $\delta^{18}O$ values is clear,

and furthermore, a two-step decrease in $\delta^{18}O$ values for both the planktonic and benthic record is notable. The initial shift to lower $\delta^{18}O$ values occurs between 14 and 12.5 ka. Thereafter, radical shifts occur from 3.69 to 2.62‰ for *C. wuellerstorfi*, 4.45 to 3.35‰ for *G. turgida*, and 4.3 to 3.44‰ for *O.umbonatus*.

Glacial to interglacial $\delta^{13}C$ amplitude shifts range from −0.8 to 0.6‰ for *C. wuellerstorfi*, −2.1 to −0.31‰ for deep infaunal *G. turgida*, and −1.7 to −0.8‰ for epifaunal shallow infaunal *Oridisalis umbonatus* (Figure 4). During MIS4, *C. wuellerstorfi* exhibits a mean $\delta^{13}C$ value of −0.45‰. In contrast, both infaunal species show lower values with averages of −0.93‰ (*G. turgida*) and −1.32‰ (*O. umbonatus*) (Figure 4). The maximum $\delta^{13}C$ shift of *O. umbonatus* occurs at the onset of MIS3 when it changes from −1.5 to −1.0‰. Throughout MIS3, *G. turgida* exhibits the most negative $\delta^{13}C$ values of the record, with a prominent shift from −0.8 to −2‰ at circa 50 ka. By contrast, *O. umbonatus* records relatively higher $\delta^{13}C$ during early MIS3 above average for MIS3 at approximately −1.26‰. *Cibicides wuellerstorfi* and *G. turgida* demonstrate relatively higher $\delta^{13}C$ values during MIS2, ranging from −0.4 to 0.4‰ and −1.0 to −0.4‰, respectively, with the former showing a shift to positive values during the latter part of MIS2 and throughout MIS1, reaching 0.6‰.

4.4. Grain Size Analysis

During MIS4 and MIS3 the mean grain size does not express large fluctuations with the exception of during 61.1–63.2 ka where it oscillates between 7.3 and 20.8 μm. Otherwise, mean grain size remains between approximately 0.4 and 15 μm with some rapid fluctuations between 65 and 60 ka. However, the end-member (EM) model reveals auxiliary detail. The particle-size distributions of the terrigenous sediment fraction in core GeoB3606-1 can best be described by three end-members (Figure 4). End-member EM1 has a modal grain size of ~3 μm, EM2 of ~10 μm, and EM3 of ~15 μm. EM1 is most dominant during late MIS4 and throughout MIS3, with EM2 being subordinate with a negligible component of EM3. Between 44 and 41 ka, a substantial shift occurs where EM2 becomes dominant, replacing EM1 and EM3 also increases. Subsequently, the dominance of EM1 returns until circa 32 ka whereby coarse particles of EM3 are most dominant until the onset of MIS2. Throughout MIS2, EM3 is of chief importance together with EM1. EM2 disappears during this stage but returns at low levels in MIS1. During MIS1 a mean grain size ranging from 13.5 to 27.9 μm is the highest of the record and the end-member model confirms a great shift toward coarse-grained sediment input evidenced from EM3 dominating this period.

4.5. Diatom Assemblages

Within the BUS, diatoms are the main contributors to the biogenic siliceous fraction. As shown by *Romero et al.* [2003], *Romero* [2010], and *Romero et al.* [2015], the GeoB3606-1 diatom record has a highly diverse assemblage with over 150 species, dominated by resting spores of *Chaetoceros* from 70 to 15 ka. Between 70 and 28 ka, the DAR exhibits highest values and strongest fluctuations in magnitude (Figures 4 and 6). Exceptionally high DAR occurs during MIS3 peaking at 55 ka with 19.7×10^8 valves $cm^{-2}\,ka^{-1}$. During MIS2 and MIS1, DAR declines to values of 9.2×10^7 to $10.6.2 \times 10^7$ and 1.2×10^6 to 9.4×10^5 valves $cm^{-2}\,ka^{-1}$, respectively. Several shifts in assemblage composition are seen, with spores of *C. debilis* and *C. dydimus* dominating the period 66–44 ka and spores of *C. affinis* and *C. compressus* being most abundant between 44 and 19 ka. Pelagic diatoms *Actinocyclus octonarius*, *Azpeitia nodulifera*, and *Coscinodiscus radiatus* and the coastal *Actinoptychus senarius* contribute to a substantial relative abundance of the assemblage from 15 ka to the late Holocene. The diatom flora can be divided into three main groups: (1) species associated with strong coastal upwelling, (2) moderate coastal upwelling, and (3) pelagic, warm waters with low-productivity conditions [*Romero et al.*, 2015]. Upwelling indicating species constitutes over 80% of the diatom assemblage throughout MIS4 to MIS2. From circa 19 ka to the present a shift in the diatomaceous flora is distinct whereby MIS1 shows a two-step change in diatom species. During the first half of MIS1, warm surface water indicators are dominant and thereafter, coastal planktic species succeed.

4.6. Bulk Geochemical Analysis

Great changes in sediment composition are recorded at site GeoB3606 (Figure 5). The $CaCO_3$ content ranges between 5 and 72% with highest values during MIS1. Total organic carbon (TOC) content ranges between 4 and 10.5%, averaging at 7.5% over the entire studied interval. MIS3 is characterized by the highest TOC content, reaching 10.5% at 45 ka, for example. TOC demonstrates a productivity shift to low (below the average of 5%) values during MIS1 whereby $CaCO_3$ is the dominant constituent. Biogenic opal levels progressively increase from <5% up to 40% during MIS4. Opal fluctuates greatly, particularly during MIS3 where values oscillate around 30% ranging between 5 and 45%. Overall, opal content is generally very high for both MIS4 and MIS3. At circa 40 ka, opal displays a relative decrease, fluctuating around 20%. Within MIS2, opal

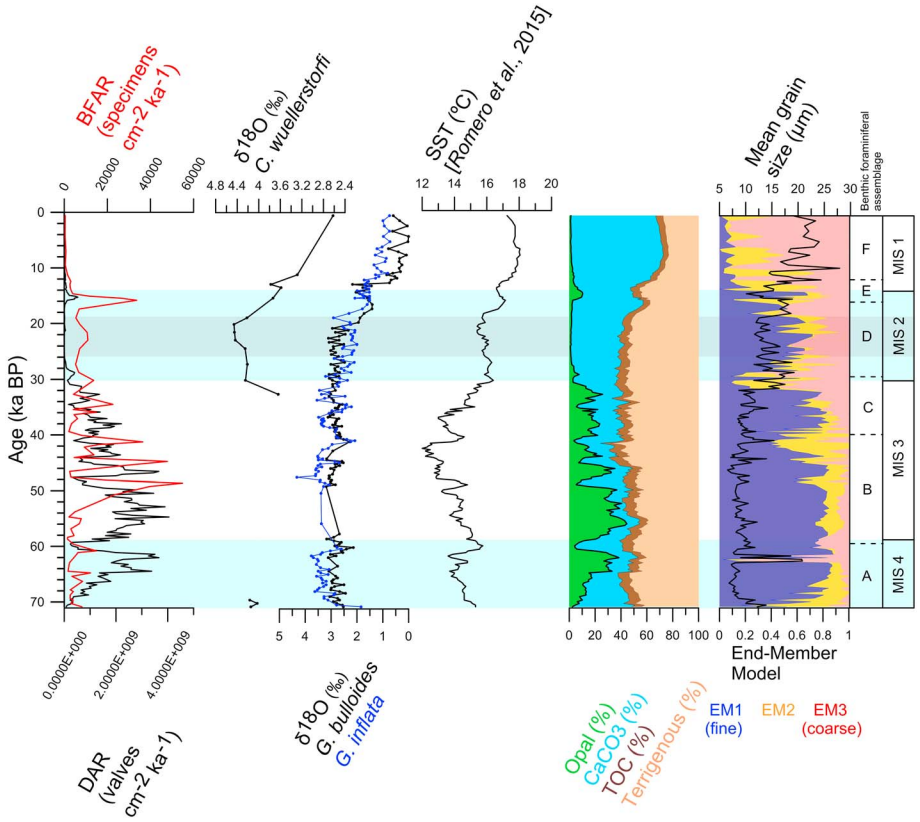

Figure 5. GeoB3606-1 downcore variation of diatom accumulation rate (valves $cm^{-2}\,ka^{-1}$); benthic foraminiferal accumulation rate (specimens $cm^{-2}\,ka^{-1}$); $\delta^{18}O$(‰) of *C. wuellerstorfi*, *G. bulloides*, and *G. inflata*; cumulative percent of biogenic opal, $CaCO_3$, and TOC; mean grain size; and proportions of end-members (EM) 1–3, where EM1 represents the fluvial component and EM2 and EM3 fine and coarse aeolian dust, respectively.

declines to low levels (<2%) with the exception of a peak at the onset and end of this period (5 and 10%, respectively). Subsequently, opal levels are deficient and less variable throughout MIS1.

5. Discussion

The high-resolution record at site GeoB3606 represents the first direct account of the coupling between the surface productivity and the benthic environment within the BUS. Based on our multiproxy approach, primary productivity intensity determines not only the benthic faunal composition but also the benthic foraminiferal abundances. The extent of this interplay between the surface and benthic environment varies depending on the hydrographical conditions. This emphasizes that the dynamics of the BUS are multifaceted, with influences of oceanographic and atmospheric processes over the course of the last 70 ka. Findings and interpretations are summarized in Table 3.

5.1. Late MIS4 70–59 ka

Within benthic foraminiferal assemblage A, the most dominant species *Eubuliminella exilis* is strikingly coupled with primary productivity (Figure 3 and Table 4). This is particularly apparent where DAR increases substantially during 66–61 ka. In this respect, during 70–66 ka and 61–60 ka, when DAR and *E. exilis* are relatively lower (e.g., <30%), *Bolivina pseudopunctata*, *Cassidulina laevigata*, *Bulimina aculeata*, and *Nonionella iridea* become more abundant (Figure 3). The rapidity in these benthic community shifts likely indicates food source to be the controlling factor. *Eubuliminella exilis* has previously been associated with pulse-like high organic input of high nutritive quality [*Caralp*, 1989; *Jannink et al.*, 1998] and is able to survive low oxygen conditions [*Pérez et al.*, 2001; *Filipsson et al.*, 2011]. Other species within this assemblage such as *N. iridea* also consume fresh organic matter [*Polovodova Asteman et al.*, 2013] but cannot tolerate such low oxygen conditions to the same extent. High relative abundance of *E. exilis* and its ability to outcompete *N. iridea* and other species during

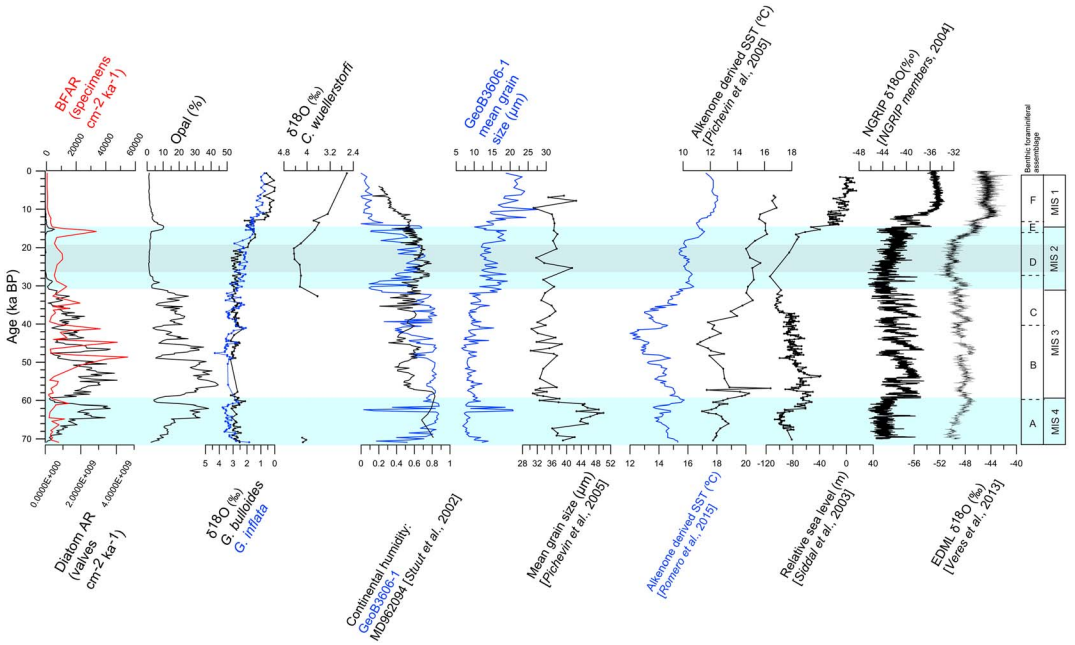

Figure 6. GeoB3606-1 downcore variation of diatom accumulation rate (valves $cm^{-2}\,ka^{-1}$), benthic foraminiferal accumulation rate (specimens $cm^{-2}\,ka^{-1}$), $\delta^{18}O$(‰) of *C. wuellerstorfi*, fine end-member model as a proxy of continental humidity from the GeoB3606-1 and MD962094 records [*Stuut et al.*, 2002], mean grain size from the GeoB3606-1 and MD962087 records [*Pichevin et al.*, 2005], alkenone-derived SST from the GeoB3606-1 and MD962087 records [*Romero et al.*, 2015; *Pichevin et al.*, 2005], relative sea level [*Siddall et al.*, 2003], NGRIP record [*North Greenland Ice Core Project members*, 2004] with the Greenland ice core chronology 2005 (GICC05) timescale down to 59.95 ka and the GICC05modelext timescale beyond 59.95 ka, and the EDML record [*Veres et al.*, 2013].

intense phytodetritus export is interpreted as signifying low oxygen conditions at the seafloor. We therefore postulate that the excessively high productivity export increased organic matter at the seafloor, which resulted in increased decomposition and oxygen consumption by bacterial respiration. This in turn decreased oxygen levels of the bottom and pore water even further in this low oxygen prone system. A similar response in coupling between the surface productivity and the benthic environment has previously been reported from studies from the upwelling system off the coast of NW Africa [*Filipsson et al.*, 2011; *McKay et al.*, 2014].

While depressions and peaks in opal are anticorrelated with $CaCO_3$, their shifts can best be explained by changes in surface productivity (opposed to dissolution, with the exception of late MIS4 and late MIS2 where planktonic foraminifera were observed at low abundance) judging by good preservation (little fragmentation) of carbonate producers from microscopy observations. High opal concentrations (>25 wt %) at site GeoB3606 potentially dilutes the signal of $CaCO_3$ due to such high export productivity of diatoms, which has been attributed to silica-rich waters of Antarctic origin [*Romero et al.*, 2003; *Romero*, 2010; *Romero et al.*, 2015]. Moreover, we can also speculate on the linkage between high-latitude climate perturbations and the frequency of the episodic DAR and opal variations. In general, during glacials the export of nutrients in the sub-Antarctic has been reported to be higher than during interglacials [*Kohfeld et al.*, 2005; *Martínez-Garcia et al.*, 2009]. In addition, enhanced phytodetritus in the South Atlantic sector has been linked to Northern Hemisphere cold events (Heinrich events) due to a latitudinal shift of the South Atlantic thermal subtropical front where enhanced vertical mixing increases nutrient content of the surface waters [*Diz and Barker*, 2015]. Occasionally, within our record, peaks in DAR coincide with colder Northern Hemisphere events as seen from the North Greenland Ice Core Project (NGRIP) record (e.g., at 66, 64.5, and 62 ka; Figure 6) and concomitant antiphase response in the Southern Hemisphere, as seen from the East Dronning Maud Land (EDML) record [*Veres et al.*, 2013] (Figure 6). This implies that the effects of the bipolar seesaw mechanism influenced latitudes up to at least the BUS region during MIS4.

At the local scale, the high surface productivity signaled by the high diatom values is in accordance with several studies from the BUS during this time interval [*Summerhayes et al.*, 1995; *Griffiths et al.*, 2013]. However, in contrast, paleoproductivity records from pelagic sites from the same area, outside the influence of chlorophyll

filaments, are not consistent with this, such as a close-by radiolarian-based record [*Jacot Des Combes and Abelmann*, 2007]. The contrast in productivity regimes between shelf and pelagic sites highlights the spatial complexity in upwelling dynamics within the BUS.

A prominent feature of late MIS4 is the dominance of fine EM1 and an absence of coarse EM3 which indicates that humid conditions were prevalent on the adjacent continent at 25°S. We interpret the high proportion of EM1 as potentially fluvially derived material; humid conditions during this time interval are consistent features of terrestrial records from the Namibia region [*Shi et al.*, 2001; *Stuut et al.*, 2002]. This conforms to the climate of MIS4 when the winter rainfall belt shifted north during glacial periods as the polar front migrated toward the equator [*Van Zinderen Bakker*, 1967; *Tyson*, 1986; *Shi et al.*, 2000; *Stuut et al.*, 2004]. This migration of climate belts is also known to promote a strengthening of the SE trade winds due to a meridional pressure gradient increase, and accordingly, upwelling intensified [*Little et al.*, 1997; *Stuut et al.*, 2002; *Pichevin et al.*, 2005]. Our interpretation of upwelling intensification during MIS4 is supported by the general higher $\delta^{18}O$ values exhibited by our planktonic *G. inflata* and *G. bulloides* record as well as the alkenone record [*Romero et al.*, 2015]; this reflects decreased sea surface temperature (SST), also consistent with other SST records from the region [*Pichevin et al.*, 2005]. Furthermore, the $\delta^{18}O$ record of our benthic stable ^{18}O isotope analyses corresponds to typical values of approximately 4‰, from MIS4 [*Hodell et al.*, 2000], suggesting large continental ice sheets and cold bottom water temperatures.

5.2. Early MIS3: 59–40 ka

The second benthic foraminiferal assemblage (B) is assigned between 59 and 40 ka. Most remarkable is the close synchronicity between the temporal distribution of *E. exilis* and DAR during early MIS3 which highlights the close correspondence between surface productivity and the benthos. As previously discussed, *E. exilis* is a taxon that exploits phytodetritus. Therefore, we propose again that the extensively high DAR is the determining factor of the benthic community whereby a threshold in DAR is crossed to the point where it degrades the bottom water oxygen content even further to the extent that it impacts the seafloor environment (Table 4). Another prominent species, *B. pseudopunctata*, further supports this interpretation [*Pérez et al.*, 2001] as well as *C. wuellerstorfi* which requires sufficient oxygen levels to thrive, is barely present at all during MIS3.

Diatom accumulation determines not only the faunal assemblage composition but also the BFAR. For some portions of the record (for example, 59–50 ka and 47.9–46 ka) a negative relationship exists between DAR (high) and BFAR (low) (Figure 3), meaning that during times of exceedingly high surface productivity, the benthic productivity is inhibited and therefore mostly only the low oxygen tolerant species survive (namely, *E. exilis*). Moreover, this negative response of the benthos occurs when DAR is over 1.4×10^9 valves $cm^{-2}\,ka^{-1}$ which we speculate to be the threshold of organic input beneficial to the benthic environment. Subsequently, as such high DAR decline, the benthic foraminiferal productivity recovers rapidly (e.g., at 48.6 ka, 44.8 ka, and 41.3 ka). We also see that the trend of DAR peaks coinciding with cold events in the NGRIP record (Figure 6) continues into MIS3. Furthermore, we see no trends in BFAR with TOC, and therefore, we stress that BFAR cannot be considered as a stand-alone proxy of primary productivity and organic export.

Based on the knowledge that modern primary productivity is enhanced at the filament front, we interpret the variation in DAR to indicate changes of the former filament front position. Therefore, we attribute the high surface productivity regime from 59 to 40 ka to increased upwelling of Si-rich waters of Antarctic origin due to the trade wind effect on the DAR; at times (56 and 54.5 ka, for example) such peaks correspond to stadials in the NGRIP record (Figure 6). Additionally, the interval of the highest DAR between 68 and 44 ka in particular matches a sea level low stand of 60–90 m lower than present day [*Siddall et al.*, 2003] (Figure 6). We speculate that a seaward migration of the coastline contributed to the displacement of the filament front over site GeoB3606-1, where upwelled waters rapidly varied between Si-rich and Si-depleted periods. However, *Siddall et al.* [2008] stated that sea level changes during MIS3 probably did not follow systematic patterns, and therefore, we do not claim that the productivity and alkenone-derived SST variability owes to rapid sea level fluctuations alone, but rather that atmospheric and hydrographic changes in the BUS changes in the BUS might have been reinforced by the effects from the sea level changes. Thus, sea level variability could act as an amplifier, further intensifying the upwelling strength during this period.

While it could be argued that the preserved productivity maximums might have been influenced by remobilization or lateral transport [*Romero*, 2010, and references therein], it has previously been

proposed that the lower slope is more strongly influenced by vertical opposed to lateral, downslope transport [*Inthorn et al*., 2006]. However, the rapid and recurrent pulses of silica and DAR can be attributed to the advection of Si-rich waters of Antarctic origin. This increased influence of Antarctic water during MIS3 has previously been deduced from the high relative abundance of the Antarctic diatom *Fragilariopsis kerguelensis* [*Romero*, 2010]. The transportation of waters from higher latitudes would require an active thermohaline circulation (THC). Theoretically, the less negative $\delta^{13}C$ values of epifaunal-shallow in-faunal species *O. umbonatus* [*Murray*, 1991] reflect ocean circulation characteristic of interglacial conditions with potential THC intensification [*Curry et al*., 1988] and a change in the dominant bottom water mass during MIS3 compared to MIS4. Despite this, oxygen levels of the bottom waters were still inhibited by excessive surface production.

In contrast, deep in-faunal *G. turgida* $\delta^{13}C$ values show the opposite trend and therefore relate to microhabitat effects as deep-dwelling taxa are more strongly $\delta^{13}C$ depleted than shallow dwellers or epifaunal species and also enhanced organic input. This increases ^{13}C-depleted carbon by increased organic matter decomposition [*McCorkle et al*., 1990, 1997]. Therefore, the largest negative $\delta^{13}C$ values of *G. turgida* during highest DAR are to be expected during early MIS3. Of additional importance, *G. turgida* occurs in low concentrations and accumulation rates during early MIS3, despite the fact that the species can withstand anoxic conditions as it has the ability to denitrify [*Risgaard-Petersen et al*., 2006; *Piña-Ochoa et al*., 2010]. Therefore, we suggest that the food source (fresh phytodetritus in the form of diatoms) subdued its abundance, opposed to the low oxygen content of the waters.

The good match between the highest contribution of highly productive coastal waters and the alkenone-based SST [*Romero et al*., 2015] indicates intense upwelling which is consistent with Mg-/Ca-based SST records of the region [*Hessler et al*., 2011]. During the sustained influence of Antarctic waters on the BUS and strong upwelling, early MIS3 is also characterized by humid conditions, particularly during 59 to 43 ka. Based on the dominance of the fine EM1 correlating with opal during MIS3, we question if the influx of fluvially transported material (particularly from the exposed shelf during sea level low stands) might have acted as an additional source of nutrients delivered to the uppermost water column overlying site GeoB3606, fueling primary productivity. Sediments delivered to the SE Atlantic Ocean by the Orange River are distributed northward by the Benguela Current [*Bluck et al*., 2007]. However, there is no evidence of freshwater diatom species in core GeoB3606-1 to support this, and therefore, the importance of fluvial transported nutrients during this time period remains an open question. Furthermore, it has been reported that not only that the Benguela Current is involved in the dispersal of clays [*Bremner and Willis*, 1993] but also that nepheloid layers related to low sea levels may affect the fine end-member proportion [*Stuut et al*., 2002]. This highlights another possible transport mechanism during early MIS3 in particular, when the variability of sea level was significantly higher than during than late MIS4 [*Siddall et al*., 2003] (Figure 6), altering the availability of fine clays from the shelf accordingly.

5.3. Late MIS3: 40–30 ka

The second foraminiferal faunal assemblage (C) identified within MIS3 occurs from 40 ka to the onset of MIS2 at 30 ka (Figure 3 and Table 4). Increased abundances of *C. laevigata* and *N. iridea* with *B. aculeata* as an important accessory species coincide with the relative decrease in *E. exilis* and DAR throughout late MIS3. We interpret this as a response to nutrient input and decreased competition of *E. exilis*. Further evidence of a benthic foraminiferal response to a change in food source is found with the rapidly fluctuating abundance of *B. pseudopunctata*, which could indicate opportunistic behavior [*Pérez et al*., 2001], and the relative increase in *U. peregrina* which feeds on refractory organic matter. While DAR is still fairly high, during late MIS3 it accumulates at approximately half the rate of early MIS3. Therefore, we note a change in pore water conditions when DAR and accordingly *E. exilis* exhibit a relative decrease clearly seen in the shift toward higher $\delta^{13}C$ values of the *G. turgida* (Figure 4). Also, as *G. turgida* is a deep infaunal species, it is most likely that its $\delta^{13}C$ values reflect changes in redox conditions in the sediment. Furthermore, a relative large general increase in oxygenation of the bottom waters remains questionable for two reasons. First, both *C. laevigata* and *B. aculeata* are abundant and can tolerate short-term hypoxic and anoxic conditions [*Nardelli et al*., 2014] and second, no dramatic shift in $\delta^{13}C$ of the *O. umbonatus* record is apparent.

We relate the shift to relatively lower DAR values from 40 to 30 ka to the decreased availability of nutrients in the waters overlying site GeoB3606-1. At times when peaks in DAR do occur (e.g., 36 and 33 ka), they tend to correspond to NGRIP stadials and the according Antarctic antiphase response, but not to the extent that low

DAR can be attributed to the reverse interhemispheric climate scenarios. Therefore, declining surface productivity was possibly caused by a decrease in Si-rich waters (Figure 5) through a seaward displacement of the upwelling front [*Romero et al*., 2015], and not by a decrease in upwelling intensity itself or direct linkages with high-latitude perturbations. We argue for the position of the filament front to be less favorable for high productivity, since strong upwelling is evidenced from coarse end-member (EM3) being more pronounced. This indicates an increased proportion of wind-transported aeolian particles compared to early MIS3 which is in agreement with another closeby grain size record [*Pichevin et al*., 2005]. This suggests not only more arid conditions, but also, we infer intensified, wind-induced upwelling. Intensified upwelling is further evidenced from the low SSTs documented by the δ^{18}O signal of planktonic foraminifera *G. bulloides* and the alkenone record of GeoB3606-1 [*Romero et al*., 2015]. This is consistent with other records obtained from 25°S [*Summerhayes et al*., 1995] as well as other archives from the BUS such as increased abundance of cold-water planktonic foraminifera *Neogloboquadrina pachyderma* [*Little et al*., 1997] and radiolarian-based studies [*Jacot Des Combes and Abelmann*, 2007]. Concurrent with our hypothesis that the position of the filament determines the local productivity levels and the response of the benthos is the interval of sea level low stand at around 40 ka [*Siddall et al*., 2003; *Rohling et al*., 2008] (Figure 6), which reinforces our speculation that the effect of low sea level is an additional underlying factor influencing the productivity dynamics here.

5.4. Early-Late MIS2 30–16 ka

Foraminiferal assemblage D is dominated by *Bulimina aculeata* with *Cassidulina laevigata* and *Nonionella iridea* as important secondary species. Accompanying species include *Bulimina mexicana* and more stable abundances of *Oridisalis umbonatus*, the latter displays more stable abundances during this time interval. All species highlight a typical setting of high organic carbon input. Therefore, in spite of low fresh phytodetritus export, food from other sources was sufficient to support benthic species that thrive on refractory organic matter such as *C. laevigata*. The dominant *C. laevigata* during MIS2 is consistent with other records from the BUS [*Schmiedl and Mackensen*, 1997] and the Angola Basin [*Van Leeuwen*, 1989]. The rapid decline in fresh phytodetritus input leads to a decline in *E. exilis*, and it is possible that the bottom water oxygen conditions improved slightly. However, while there is an albeit minor but noticeable increase (a few individuals) of *Cibicides wuellerstorfi*, the BFAR does not exhibit a great increase during MIS2. Therefore, we infer that bottom water oxygen conditions remained low. Owing to the low DAR, changes in surface water dynamics must have been responsible for this benthic foraminiferal community response.

Besides the benthic foraminiferal assemblage composition, *C. wuellerstorfi* δ^{13}C values also potentially document oceanographic changes. We infer that this could be an accompanying underlying reason for a relative recovery in bottom water conditions. However, since the LGM is typically characterized by hampered ocean circulation, in general [*Bitz et al*., 2007], we call into question whether this is a true signal of a deep ocean circulation shift. More likely, it is a reflection of the rapid decline in export productivity being the major influence on bottom water conditions and the benthic life it supports.

The decline in export productivity can be related to a further offshore migration of the upwelling filament during MIS2. An equatorward shift of the Southern Hemisphere westerlies and increased trade wind strength could have contributed to pushing the filament front into more open waters, away from site GeoB3606-1, during MIS2. Sea level low stand of at least 125 m below present day during the LGM [*Waelbroeck et al*., 2002] may have amplified this offshore filament migration and also produced increased shelf-to-slope lithogenic transport due to exposure of the shelf, here evidenced by the fine EM1. Of additional importance, we also highlight the increased importance of the increase in mean grain size and also coarsest EM3 which replaces the finer aeolian EM2 (Figure 5). From this increase in coarser grain size which corresponds to other grain size records of the region [*Pichevin et al*., 2005], in conjunction with the alkenone-derived SSTs, our record certainly suggests that MIS2 is characterized by increased wind strength and according upwelling intensity. Stronger upwelling caused by an equatorward shift of Southern Hemisphere westerlies which intensified the trade winds is characteristic of glacial periods [*Abrantes et al*., 1994; *Abrantes*, 2000; *Berger and Wefer*, 2002b]. Nevertheless, during MIS2, no distinct decrease in SST is discerned from the planktonic δ^{18}O values or the alkenone record [*Romero et al*., 2015]. Thus, we assume that although trade wind strength was intensified, it was not sufficient to increase upwelling strength directly over site GeoB3606.

Deviations in the position of the upwelling filament have previously been reported in the BUS [*Mollenhauer et al*., 2002]. When we compare our record to *Mollenhauer et al*. [2002] who investigated several cores from

the Namibian continental slope, it underscores the extent to which the position of the upwelling centers affect productivity spatially within the BUS. Several records from upwelling sites postulate lower glacial productivity with a decline in the supply of diatoms and other siliceous organisms [*Diester-Haass et al*., 1988; *Anderson et al*., 2001]. Our results are in agreement with this as opal levels, and hence, diatoms decline during MIS2, in particular during the LGM. Such decline of MIS2 primary production has previously been ascribed to an equatorward shift of the trade winds that were not favorable for upwelling [*Little et al*., 1997]. Hence, we underline that TOC remains high throughout the period and $CaCO_3$ content exhibits a relative increase, which reflects major changes in nutrient availability and source. In tandem with this and the close correspondence between low opal content and DAR, we suggest that the opal content is also potentially more stifled by the more sluggish ocean circulation characteristic of the LGM, meaning less injection of silica-rich Antarctic waters.

5.5. Termination of MIS2 and Onset of MIS1: 16–12 ka

Benthic foraminiferal assemblage E is dominated by *Bulimina aculeata* (Figure 3 and Table 4) which responds quickly to fresh organic matter [*Kitazato et al*., 2001]. In this respect, it is interesting to note that *Eubuliminella exilis* does not recover in abundance to dominate the assemblage during the small peak in DAR at 16–14 ka. Possibly, this is due to bottom water oxygenation not declining to previously low levels where *E. exilis* could outcompete all other species during MIS3.

As the rapid decrease in BFAR during this time interval coincides with a progressive decrease in DAR, we infer that the benthos is tightly coupled with the surface productivity (Figure 3). Meanwhile, the inflow of Antarctic waters into the BUS is indicated by the peak in biogenic opal increase and lower SSTs demonstrated by the planktonic $\delta^{18}O$ foraminiferal record and alkenone record [*Romero et al*., 2015]. This cooler interval is consistent with other nearby Mg/Ca-derived SST records [*Farmer et al*., 2005] and alkenone-based SST records [*Kim et al*., 2002]. The timing of this is consistent with the occurrence of the Antarctic Cold Reversal (ACR; Figure 6) at 14.5–12.8 ka [*Blunier et al*., 1997, 1998], Southern Ocean decreases in SST [*Barker et al*., 2009], and a northward displacement of the Southern Hemisphere westerlies [*Ljung et al*., 2015]. The cooling associated with the ACR is documented in terrestrial records from southern Africa [*Gasse*, 2000; *Holmgren et al*., 2003] as well as humid conditions here inferred from fine EM1 [*Shi et al*., 1998, 2000]. Of further note is the *C. wuellerstorfi* $\delta^{13}C$ values of $>0.04‰$ signifying circumpolar deep water, reflecting a balance between NADW and deep waters formed in the Southern Ocean [*Charles and Fairbanks*, 1992]. To compliment this finding, *B. aculeata* has been found to be associated with circumpolar deep water [*Mead and Kennett*, 1987]. Therefore, we interpret this shift in $\delta^{13}C$ and benthic faunal composition to confirm ocean circulation changes and hence an enhanced ocean conveyor during the ACR. The trigger for strengthened THC at this time has previously been attributed to the injection of freshwater perturbations by a surge of the Antarctic Ice Sheet [*Weaver et al*., 2003]. Therefore, potentially, the presence of nutrient-depleted NADW and decrease in fresh phytodetritus export during the latter half of this assemblage inhibited the BFAR.

After the ACR at 12.8 ka, *B. aculeata* continues to be dominant but other species previously of low abundance in the core increase, such as *E. exigua*. Concurrently, both alkenone and *G. bulloides* and *G. inflata* $\delta^{18}O$-based SSTs began to increase, coinciding with aridity inferred from the abrupt switch to dominance in coarse EM3 input, during warmer conditions. Hence, we interpret this to be the onset of the Antarctic Holocene optimum in MIS1 (Figure 6).

5.6. MIS1: the Holocene 12–0 ka

Owing to the appearance of benthic foraminiferal species which were previously less abundant (such as shallow in-faunal species *Fursenkoina rotundata* and epifaunal species *Gyroidinoides soldanii*) alongside the demise of both *E. exilis* and *B. aculeata*, we here highlight the foremost benthic community shift within the GeoB3606-1 record (Figure 3 and Table 4). In particular, this sixth assemblage shows dramatic increase in opportunistic *E. exigua*. A similar shift toward an assemblage being highly abundant in this species has previously been reported by *Schmiedl and Mackensen* [1997] in a close-by core from 24°S. They attributed this to high seasonality of phytodetritus input. In addition, epifaunal-shallow in-faunal *O. umbonatus* abundance increases markedly which resides in more oxygenated bottom water where a low flux of highly degraded organic matter is sustained [*Mackensen*, 1985]. We interpret this faunal shift to indicate that oxygen concentration at the bottom and in the pore waters were not as low as previously when DAR suppressed

it, but waters were still far from well oxygenated. Overall, much like the decline in DAR during MIS2, foraminiferal assemblage F highlights the implications of changes in food source and oxygen availability. However, in contrast to MIS2, the BFAR is exceptionally low (on average 716 specimens $cm^{-2}\,ka^{-1}$) which we assume is a result of major changes in nutrient availability in the surface waters due to hydrographical-related shifts and resultant low primary productivity export during the Holocene.

Hydrographical changes in the BUS are documented by not only the lower DAR and TOC (Figure 5) but also by the diatom composition that demonstrates a dominance of warm, pelagic waters and a low contribution of upwelling waters [*Romero et al*., 2015]. We therefore conclude that upwelling was more restricted during the last 12 ka. This lower productivity at site GeoB3606 may be augmented by higher sea level retracting the locality of the upwelling filament. In addition to sea level playing a role in determining filament locality and the nutrient provision to site GeoB3606, eddy-induced offshore transport could potentially lead to the hindering of nutrients being upwelled resulting in much lower export of productivity. *Gruber et al*. [2011] recently reported that eddies can have a suppressing effect upon biological production in eastern boundary current systems.

The proxy variables representing upwelling intensity display contrasting patterns during the Holocene, as the dominance of the coarse EM3 and highest mean grain sizes of the record implies increased wind strength and according carrying capacity, whereas the planktonic $\delta^{18}O$ values demonstrate considerably warmer conditions, indicating reduced upwelling (Figure 5). Thus, we infer weaker upwelling strength and presume that the end-member model result solely implies arid conditions of the adjacent land mass. This climatic shift in our record fits well with previously documented studies of northern, southern, and equatorial Africa [*Schneider et al*., 1997; *Kirst et al*., 1999; *Marchant and Hooghiemstra*, 2004; *Dupont*, 2006] and is also compatible with deglacial warming of the Arctic and Antarctic ice records [*Johnsen et al*., 1972, 1992; *Veres et al*., 2013] (Figure 6). It has been proposed that a farther northward movement of the Intertropical Convergence Zone (ITCZ) probably led to this, resulting in a reduction of water vapor supply to southern subtropical Africa [*Shi et al*., 2000].

Furthermore, during the deglacial shift in the ITCZ which promotes reorganizations of the Southern Hemisphere westerlies [*Toggweiler et al*., 2006], the Southern Hemisphere subtropical front incurred the reactivation of the oceanic thermohaline circulations and thus of the Agulhas Current [*Gasse*, 2000; *Golledge et al*., 2014]. Agulhas leakage maxima into the southern BUS were a persistent feature of terminations [*Peeters et al*., 2004; *Scussolini et al*., 2015]. The main characteristic of this oceanographic feature is increased SST [*Gordon et al*., 1992] which is consistent with our planktonic $\delta^{18}O$ data and further supported by the abundance of a more pelagic-related diatom flora [*Romero et al*., 2015]. This shift in climate and hydrography potentially explains the surface productivity regime shift to one dominated by calcareous producers.

The abrupt transition in climate and upwelling characteristics of MIS1 were accompanied by deep oceanographic changes at site GeoB3606 as suggested by the shift in epifaunal benthic $\delta^{13}C$ values. We postulate that shifts in water masses bathing site GeoB3606 also influenced the very notable shift in species composition of the benthic foraminiferal assemblage. Highest values of $\delta^{13}C$ of epifaunal *C. wuellerstorfi* ($>0.5‰$) match other records from this region and have been interpreted to show an enhanced advection of NADW into the SE subtropical Atlantic during this interglacial period [*Schmiedl and Mackensen*, 1997; *Ninnemann et al*., 1999]. While reactivation in the THC would enhance ventilation of the ocean floor, NADW is known to be nutrient deficient and therefore does not compensate for the decline in nutrient export from the surface waters.

6. Conclusion

Our downcore multiproxy reconstruction reveals significant changes in the benthic environment due to changes in productivity export in the Benguela Upwelling System during the last 70 ka, covering late MIS4 to MIS1. Our study represents the first late Quaternary benthic foraminiferal record linked directly to diatom productivity in this particular upwelling region, which enabled us to identify a tight coupling between the surface and bottom water environment.

Overall, we observe several benthic foraminiferal assemblages throughout the past 70 ka in response to changes in food source and benthic environmental conditions. The complex interactions of large-scale

climatic and hydrographic changes upon this coupling are well recorded, and we conclude that upwelling intensity, filament locality, and ocean circulation had significant implications for productivity and accordingly the benthic environment. Changes in upwelling intensity are not necessarily expressed as simply glacial-interglacial conditions within the BUS. While occasionally, fluctuations in primary productivity related to opal flux seem to be related to effects of the bipolar seesaw mechanism during MIS4-MIS2, with productivity peaks during Northern Hemisphere stadials, more regional changes in upwelling dynamics and hydrography play an important role for the productivity variability and according benthic response at site GeoB3606-1.

Perhaps the most striking aspect of this work is the extraordinarily tight correlation between diatom accumulation rate and the abundance of low oxygen tolerant benthic foraminiferal species *Eubuliminella exilis*. In particular, within MIS4 and MIS3 this relationship highlights the concept of thresholds with regard to high diatomaceous export triggering low oxygen conditions at the seafloor and corresponding low benthic foraminiferal productivity. From the low benthic productivity during highest diatom accumulations we stress the importance of engaging caution when considering benthic foraminiferal accumulation rate as a proxy for past export productivity.

However, when we compare our results to other data from the region, we have indications that there is a strong spatiotemporal complexity in upwelling and productivity dynamics in the BUS. In conclusion, this complex of variable processes and dynamics controls the benthos across eastern boundary current systems.

Acknowledgments

The core repository at MARUM is acknowledged for providing access to samples of core GeoB3606-1. We thank R. Søraas and U. Ninneman for performing stable O and C isotope measurements (Bjerknes Centre, University of Bergen, Norway), C. Lehnen for undertaking grain size analysis with assistance and organization from J. Titschack (MARUM, University of Bremen), and M. Rundgren for radiocarbon analysis (Lund University, Sweden). Much gratitude goes to V. Brüchert, O. Hermelin, B.C. Lougheed, and J.-H. Kim for their insightful discussions. Critical comments from two anonymous reviewers greatly improved the manuscript. This research was funded by the Crafoord Foundation (20100547), the Lund University Centre for Studies of Carbon Cycle and Climate Cycle Interactions (LUCCI), Kungl. Fysiografiska Sällskapet i Lund, and the ClimBEco Graduate Research School, Lund University. H.L.F acknowledges support from the Swedish Research Council VR (621-2011-5090). Data are available in the database www.pangeaea.de.

References

Abrantes, F. (2000), 200 000 yr diatom records from Atlantic upwelling sites reveal maximum productivity during LGM and a shift in phytoplankton community structure at 185 000 yr, *Earth Planet. Sci. Lett.*, *176*(1), 7–16.

Abrantes, F., K. Winn, and M. Sarnthein (1994), Late Quaternary paleoproductivity variations in the NE and equatorial Atlantic: Diatom and Corg evidence, in *Carbon Cycling in the Glacial Ocean: Constraints on the Ocean's Role in Global Change*, edited by R. Zahn et al., pp. 425–441, Springer, Berlin Heidelberg.

Anderson, P. A., C. D. Charles, and W. H. Berger (2001), Walvis Paradox confirmed for the early Quaternary at the southern end of the Namibia upwelling system, ODP Site 1085, in *Proceedings of the Ocean Drilling Program Scientific Results*, vol. 175, edited by G. Wefer, W. H. Berger, and C. Richter, pp. 1–31, Ocean Drilling Program, College Station, Tex.

Bailey, G. W. (1991), Organic carbon flux and development of oxygen deficiency on the modern Benguela continental shelf south of 22°S: Spatial and temporal variability, in *Modern and Ancient Continental Shelf Anoxia*, edited by R. V. Tyson and T. H. Pearson, *Geol. Soc. London Spec. Publ.*, 171–183.

Bard, E. (1988), Correction of accelerator mass spectrometry ^{14}C ages measured in planktonic foraminifera: Paleoceanographic implications, *Paleoceanography*, *3*(6), 635–645.

Barker, S., P. Diz, M. J. Vautravers, J. Pike, G. Knorr, I. R. Hall, and W. S. Broecker (2009), Interhemispheric Atlantic seesaw response during the last deglaciation, *Nature*, *457*(7233), 1097–1102.

Berger, W. H., and G. Wefer (1996), Central themes of South Atlantic circulation, in *The South Atlantic: Present and Past Circulation*, edited by G. Wefer et al., pp. 1–11, Springer, Berlin.

Berger, W. H., and G. Wefer (2002a), On the reconstruction of upwelling history: Namibia upwelling in context, *Mar. Geol.*, *180*(1–4), 3–28.

Berger, W. H., and G. Wefer (2002b), Upwelling history of the Benguela-Namibia system: A synthesis of Leg 175 results, in *Proceedings of the Ocean Drilling Program Scientific Results*, vol. 175, edited by G. Wefer, W. H. Berger, and C. Richter, pp. 1–103, Ocean Drilling Program, College Station, Tex.

Bitz, C. M., J. C. H. Chiang, W. Cheng, and J. J. Barsugli (2007), Rates of thermohaline recovery from freshwater pulses in modern, Last Glacial Maximum, and greenhouse warming climates, *Geophys. Res. Lett.*, *34*, L07708, doi:10.1029/2006GL029237.

Bleil, U., and Cruise Participants (1996), Report and preliminary results of METEOR Cruise 34/1 Cape Town-Walvis Bay, 03.01.96-26.01.96, 1–129 pp, Universität Bremen.

Bluck, B. J., J. D. Ward, J. Cartwright, and R. Swart (2007), The Orange River, southern Africa: An extreme example of a wave-dominated sediment dispersal system in the South Atlantic Ocean, *J. Geol. Soc.*, *164*, 341–351.

Blunier, T., J. Schwander, B. Stauffer, T. Stocker, A. Dällenbach, A. Indermühle, J. Tschumi, J. Chappellaz, D. Raynaud, and J. M. Barnola (1997), Timing of the Antarctic cold reversal and the atmospheric CO_2 increase with respect to the Younger Dryas event, *Geophys. Res. Lett.*, *24*(21), 2683–2686.

Blunier, T., et al. (1998), Asynchrony of Antarctic and Greenland climate change during the last glacial period, *Nature*, *394*, 739–743.

Bremner, J. M., and J. P. Willis (1993), Mineralogy and geochemistry of the clay fraction of sediments from the Namibian continental margin and the adjacent hinterland, *Mar. Geol.*, *115*, 85–116.

Brüchert, V., M. E. Pérez, and C. B. Lange (2000), Coupled primary production, benthic foraminiferal assemblage, and sulfur diagenesis in organic-rich sediments of the Benguela upwelling system, *Mar. Geol.*, *163*(1–4), 27–40.

Caralp, M. H. (1989), Abundance of *Bulimina exilis* and *Melonis barleeanum*: Relationship to the quality of marine organic matter, *Geo Mar. Lett.*, *9*(1), 37–43.

Charles, C. D., and R. G. Fairbanks (1992), Evidence from Southern Ocean sediments for the effect of North Atlantic deep-water flux on climate, *Nature*, *355*(6359), 416–419.

Clark, P. U., A. S. Dyke, J. D. Shakun, A. E. Carlson, J. Clark, B. Wohlfarth, J. X. Mitrovica, S. W. Hostetler, and A. M. McCabe (2009), The Last Glacial Maximum, *Science*, *325*(5941), 710–714.

Copenhagen, W. J. (1953), The periodic mortality of fish in the Walvis region: A phenomenon within the Benguela Current, *Invest. Rep. Div. Fish. South Afr.*, *14*, 1–35.

Corliss, B. H., and S. Emerson (1990), Distribution of Rose Bengal stained benthic foraminifera from the Nova Scotia continental margin and Gulf of Maine, *Deep-Sea Res.*, *37*, 381–400.
Curry, W. B., J. C. Duplessy, L. D. Labeyrie, and N. J. Shackleton (1988), Changes in the distribution of $\delta^{13}C$ of deep water ΣCO_2 between the Last Glaciation and the Holocene, *Paleoceanography*, *3*(3), 317–341.
Dewar, G., P. J. Reimer, J. Sealy, and S. Woodborne (2012), Late-Holocene marine radiocarbon reservoir correction (ΔR) for the west coast of South Africa, *Holocene*, *22*(12), 1481–1489.
Diester-Haass, L. (1985), Late Quaternary sedimentation on the Eastern Walvis Ridge, SE Atlantic, *Mar. Geol.*, *65*(1/2), 145–189.
Diester-Haass, L., K. Heine, P. Rothe, and H. Schrader (1988), Late Quaternary history of continental climate and the Benguela Current off South West Africa, *Palaeogeogr. Palaeoclimatol. Palaeoecol.*, *65*(1–2), 81–91.
Diz, P., and S. Barker (2015), Linkages between rapid climate variability and deep-sea benthic foraminifera in the deep Subantarctic South Atlantic during the last 95 kyr, *Paleoceanography*, *30*, 601–611, doi:10.1002/2015PA002784.
Duncombe Rae, C. M., F. A. Shillington, J. J. Agenbag, J. Taunton-Clark, and M. L. Gründlingh (1992), An Agulhas ring in the South Atlantic Ocean and its interaction with the Benguela upwelling frontal system, *Deep Sea Res., Part A*, *39*(11–12), 2009–2027.
Dupont, L. M. (2006), Late Pliocene vegetation and climate in Namibia (southern Africa) derived from palynology of ODP Site 1082, *Geochem. Geophys. Geosyst.*, *7*, Q05007, doi:10.1029/2005GC001208.
Farmer, E. C., P. B. deMenocal, and T. M. Marchitto (2005), Holocene and deglacial ocean temperature variability in the Benguela upwelling region: Implications for low-latitude atmospheric circulation, *Paleoceanography*, *20*, PA2018, doi:10.1029/2004PA001049.
Filipsson, H. L., O. E. Romero, J.-B. W. Stuut, and B. Donner (2011), Relationships between primary productivity and bottom-water oxygenation off northwest Africa during the last deglaciation, *J. Quat. Sci.*, *26*(4), 448–456.
Gasse, F. (2000), Hydrological changes in the African tropics since the Last Glacial Maximum, *Quat. Sci. Rev.*, *19*(1–5), 189–211.
Golledge, N. R., L. Menviel, L. Carter, C. J. Fogwill, M. H. England, G. Cortese, and R. H. Levy (2014), Antarctic contribution to meltwater pulse 1A from reduced Southern Ocean overturning, *Nat. Commun.*, *5*, doi:10.1038/ncomms6107.
Gordon, A. L., R. F. Weiss, W. M. Smethie Jr., and M. J. Warner (1992), Thermocline and intermediate water communication between the South Atlantic and Indian Oceans, *J. Geophys. Res.*, *97*, 7223–7240.
Griffiths, J. D., S. Barker, K. R. Hendry, D. J. R. Thornalley, T. van de Flierdt, I. R. Hall, and R. F. Anderson (2013), Evidence of silicic acid leakage to the tropical Atlantic via Antarctic Intermediate Water during Marine Isotope Stage 4, *Paleoceanography*, *28*, 307–318, doi:10.1002/palo.20030.
Gruber, N., Z. Lachkar, H. Frenzel, P. Marchesiello, M. Munnich, J. C. McWilliams, T. Nagai, and G.-K. Plattner (2011), Eddy-induced reduction of biological production in eastern boundary upwelling systems, *Nat. Geosci.*, *4*(11), 787–792.
Hammer, Ø., D. A. T. Harper, and P. D. Ryan (2001), PAST: Paleontological Statistics software package for education and data analysis, *Palaeontol. Electron.*, *4*(1), 9.
Heinrich, S., K. A. F. Zonneveld, T. Bickert, and H. Willems (2011), The Benguela upwelling related to the Miocene cooling events and the development of the Antarctic Circumpolar Current: Evidence from calcareous dinoflagellate cysts, *Paleoceanography*, *26*, PA3209, doi:10.1029/2010PA002065.
Hessler, I., S. Steinke, J. Groeneveld, L. Dupont, and G. Wefer (2011), Impact of abrupt climate change in the tropical southeast Atlantic during Marine Isotope Stage (MIS) 3, *Paleoceanography*, *26*, PA4209, doi:10.1029/2011PA002118.
Hodell, D. A., C. D. Charles, and U. S. Ninnemann (2000), Comparison of interglacial stages in the South Atlantic sector of the southern ocean for the past 450 kyr: Implications for Marine Isotope Stage (MIS) 11, *Global Planet. Change*, *24*(1), 7–26.
Holmgren, K., J. A. Lee-Thorp, G. R. J. Cooper, K. Lundblad, T. C. Partridge, L. Scott, R. Sithaldeen, A. Siep Talma, and P. D. Tyson (2003), Persistent millennial-scale climatic variability over the past 25,000 years in Southern Africa, *Quat. Sci. Rev.*, *22*(21–22), 2311–2326.
Inthorn, M., T. Wagner, G. Scheeder, and M. Zabel (2006), Lateral transport controls distribution, quality, and burial of organic matter along continental slopes in high-productivity areas, *Geology*, *34*(3), 205–208.
Jacot Des Combes, H., and A. Abelmann (2007), A 350-ky radiolarian record off Lüderitz, Namibia—Evidence for changes in the upwelling regime, *Mar. Micropaleontol.*, *62*(3), 194–210.
Jannink, N. T., W. J. Zachariasse, and G. J. Van der Zwaan (1998), Living (Rose Bengal stained) benthic foraminifera from the Pakistan continental margin (northern Arabian Sea), *Deep Sea Res., Part I*, *45*(9), 1483–1513.
Johnsen, S. J., W. Dansgaard, H. B. Clausen, and C. C. Langway (1972), Oxygen isotope profiles through the Antarctic and Greenland ice sheets, *Nature*, *235*(5339), 429–434.
Johnsen, S. J., H. B. Clausen, W. Dansgaard, K. Fuhrer, N. Gundestrup, C. U. Hammer, P. Iversen, J. Jouzel, B. Stauffer, and J. P. Steffensen (1992), Irregular glacial interstadials recorded in a new Greenland ice core, *Nature*, *359*(6393), 311–313.
Jones, R. W. (1994), *The Challenger Foraminifera*, Oxford Univ. Press, Oxford.
Kirst, G. J., R. R. Schneider, P. J. Muller, I. von Storch, and G. Wefer (1999), Late Quaternary temperature variability in the Benguela Current system derived from alkenones, *Quat. Res.*, *52*(1), 92–103.
Kitazato, H., H. Nomaki, P. Heinz, and T. Nakatsuka (2001), The role of benthic foraminifera in deep-sea food webs at the sediment-water interface: Results from in situ feeding experiments in Sagami Bay, *Front. Res. Earth Evol.*, *1*, 227–232.
Kohfeld, K. E., C. L. Quéré, S. P. Harrison, and R. F. Anderson (2005), Role of marine biology in glacial-interglacial CO_2 cycles, *Science*, *308*(5718), 74–78.
Lamont, T., R. G. Barlow, and M. S. Kyewalyanga (2014), Physical drivers of phytoplankton production in the southern Benguela upwelling system, *Deep Sea Res., Part I*, *90*, 1–16.
Lange, C. B., W. H. Berger, H. L. Lin, G. Wefer, and Shipboard Scientific Party Leg 175 (1999), The early Matuyama Diatom Maximum off SW Africa, Benguela Current System (ODP Leg 175), *Mar. Geol.*, *161*, 93–114.
Levin, L. A., W. Ekau, A. J. Gooday, F. Jorissen, J. J. Middelburg, S. W. A. Naqvi, C. Neira, N. N. Rabalais, and J. Zhang (2009), Effects of natural and human-induced hypoxia on coastal benthos, *Biogeosciences*, *6*(10), 2063–2098.
Lisiecki, L. E., and M. E. Raymo (2005), A Pliocene-Pleistocene stack of 57 globally distributed benthic $\delta^{18}O$ records, *Paleoceanography*, *20*, PA1003, doi:10.1029/2004PA001071.
Little, M. G., R. R. Schneider, D. Kroon, B. Price, T. Bickert, and G. Wefer (1997), Rapid palaeoceanographic changes in the Benguela Upwelling System for the last 160,000 years as indicated by abundances of planktonic foraminifera, *Palaeogeogr. Palaeoclimatol. Palaeoecol.*, *130*(1–4), 135–161.
Ljung, K., S. Holmgren, M. Kylander, J. Sjolte, N. Van der Putten, M. Kageyama, C. T. Porter, and S. Björck (2015), The last termination in the central South Atlantic, *Quat. Sci. Rev.*, *123*, 193–214.
Loeblich, A. R., and H. Tappan (1987), *Foraminiferal Genera and Their Classification*, pp. 1–212, Van Nostrand Reinhold, New York.
Lutjeharms, J. R. E., and J. M. Meeuwis (1987), The extent and variability of South-East Atlantic upwelling, *South Afr. J. Mar. Sci.*, *5*(1), 51–62.
Lutjeharms, J. R. E., and P. L. Stockton (1987), Kinematics of the upwelling front off southern Africa, *South Afr. J. Mar. Sci.*, *5*(1), 35–49.
Mackensen, A. (1985), *Verbreitung und Umwelt Benthischer Foraminiferen in der Norwegischen See*, Univ. of Kiel Germany, Germany.

Mackensen, A., G. Schmiedl, J. Harloff, and M. Giese (1995), Deep-sea foraminifera in the South Atlantic Ocean: Ecology and assemblage generation, *Micropaleontology*, *41*, 342–358.
Marchant, R., and H. Hooghiemstra (2004), Rapid environmental change in African and South American tropics around 4000 years before present: A review, *Earth Sci. Rev.*, *66*(3–4), 217–260.
Martínez-Garcia, A., A. Rosell-Melé, W. Geibert, R. Gersonde, P. Masqué, V. Gaspari, and C. Barbante (2009), Links between iron supply, marine productivity, sea surface temperature, and CO_2 over the last 1.1 Ma, *Paleoceanography*, *24*, PA1207, doi:10.1029/2008PA001657.
McCartney, M. S. (1977), Subantarctic Mode Water, in *A Voyage of Discovery: George Deacon 70th Anniversary*, edited by M. Angel, pp. 103–119, Pergamon Press, Oxford.
McCorkle, D. C., L. D. Keigwin, B. H. Corliss, and S. R. Emerson (1990), The influence of microhabitats on the carbon isotopic composition of deep-sea benthic foraminifera, *Paleoceanography*, *5*, 161–185.
McCorkle, D. C., B. H. Corliss, and C. A. Farnham (1997), Vertical distributions and stable isotopic compositions of live (stained) benthic foraminifera from the North Carolina and California continental margins, *Deep Sea Res., Part I*, *44*(6), 983–1024.
McKay, C. L., H. L. Filipsson, O. E. Romero, J.-B. W. Stuut, and B. Donner (2014), Pelagic–benthic coupling within an upwelling system of the subtropical northeast Atlantic over the last 35 ka BP, *Quat. Sci. Rev.*, *106*, 299–315.
Mead, G. A., and J. P. Kennett (1987), The distribution of recent benthic foraminifera in the Polar Front region, southwest Atlantic, *Mar. Micropaleontol.*, *11*(4), 343–360.
Mollenhauer, G., R. R. Schneider, P. J. Müller, V. Spieß, and G. Wefer (2002), Glacial/interglacial variability in the Benguela upwelling system: Spatial distribution and budgets of organic carbon accumulation, *Global Biogeochem. Cycles*, *16*(4), 1134, doi: 10.1029/2001GB001488.
Mollenhauer, G., T. I. Eglinton, N. Ohkouchi, R. R. Schneider, P. J. Müller, P. M. Grootes, and J. Rullkötter (2003), Asynchronous alkenone and foraminifera records from the Benguela Upwelling System, *Geochim. Cosmochim. Acta*, *67*(12), 2157–2171.
Monteiro, P. M. S., and A. K. van der Plas (Eds) (2006), *Low Oxygen Water (LOW) Variability in the Benguela System: Key Processes and Forcing Scales Relevant to Forecasting in Benguela—Predicting a Large Marine Ecosystem*, pp. 71–90, Elsevier, Amsterdam.
Müller, A. A., V. Mohrholz, and M. Schmidt (2013), The circulation dynamics associated with a northern Benguela upwelling filament during October 2010, *Cont. Shelf Res.*, *63*, 59–68.
Murray, J. W. (1991), *Ecology and Palaeoecology of Benthic Foraminifera*, Longman Scientific and Technical, Harlow, U. K.
Nardelli, M. P., C. Barras, E. Metzger, A. Mouret, H. L. Filipsson, F. Jorissen, and E. Geslin (2014), Experimental evidence for foraminiferal calcification under anoxia, *Biogeosciences*, *11*(14), 4029–4038.
Ninnemann, U. S., C. D. Charles, and D. A. Hodell (1999), Origin of global millennial scale climate events: Constraints from the Southern Ocean deep sea sedimentary record, in *Mechanisms of Global Climate Change*, edited by P. U. Clark, R. S. Webb, and L. D. Keigwin, pp. 99–112, AGU, Washington, D. C.
North Greenland Ice Core Project members (2004), North Greenland Ice Core Project oxygen isotope data IGBP PAGES/World Data Center for Paleoclimatology Data Contribution Series # 2004–059. NOAA/NGDC Paleoclimatology Program, Boulder Colo.
Oberhänsli, H. (1991), Upwelling signals at the northeastern Walvis Ridge during the past 500,000 years, *Paleoceanography*, *6*, 53–71.
Peeters, F. J. C., R. Acheson, G.-J. A. Brummer, W. P. M. de Ruijter, R. R. Schneider, G. M. Ganssen, E. Ufkes, and D. Kroon (2004), Vigorous exchange between the Indian and Atlantic oceans at the end of the past five glacial periods, *Nature*, *430*(7000), 661–665.
Pérez, M. E., C. D. Charles, and W. H. Berger (2001), Late Quaternary productivity fluctuations off Angola: Evidence from benthic foraminifera, Site 1079, in *Proceedings of the Ocean Drilling Program, Scientific Results*, vol. 175, edited by G. Wefer and W. H. Berger, pp. 1–19, Ocean Drilling Program, College Station, Tex.
Pichevin, L., P. Martinez, P. Bertrand, R. Schneider, J. Giraudeau, and K. Emeis (2005), Nitrogen cycling on the Namibian shelf and slope over the last two climatic cycles: Local and global forcings, *Paleoceanography*, *20*, PA2006, doi:10.1029/2004PA001001.
Pieterse, F., and D. C. van der Post (1967), Oceanographical conditions associated with red tides and fish mortalities in the Walvis Bay region, in *Investigational Report of the Administration of South West Africa Marine Research Laboratory*, vol. 14, pp. 1–125 .
Piña-Ochoa, E., S. Høgslund, E. Geslin, T. Cedhagen, N. P. Revsbech, L. P. Nielsen, M. Schweizer, F. Jorissen, S. Rysgaard, and N. Risgaard-Petersen (2010), Widespread occurrence of nitrate storage and denitrification among Foraminifera and *Gromiida*, *Proc. Natl. Acad. Sci. U.S.A.*, *107*(3), 1148–1153.
Polovodova Asteman, I., K. Nordberg, and H. L. Filipsson (2013), The Little Ice Age: Evidence from a sediment record in Gullmar Fjord, Swedish west coast, *Biogeosciences*, *10*(3), 1275–1290.
Prins, M. A., and G. J. Weltje (1999), End-member modeling of siliciclastic grain-size distributions: The Late Quaternary record of eolian and fluvial sediment supply to the Arabian Sea and its paleoclimatic significance, in *Numerical Experiments in Stratigraphy: Recent Advances in Stratigraphic and Sedimentologic Computer Simulations*, *SEPM Spec. Publ.*, vol. 62, edited by J. Harbaugh et al., pp. 91–111, Society for Sedimentary Geology, Oklahoma.
Reimer, P. J., et al. (2013), IntCal13 and Marine13 radiocarbon age calibration curves 0–50,000 years cal BP, *Radiocarbon*, *55*(4), 1869–1887.
Risgaard-Petersen, N., et al. (2006), Evidence for complete denitrification in a benthic foraminifer, *Nature*, *443*(7107), 93–96.
Rohling, E. J., K. Grant, C. Hemleben, M. Kucera, A. P. Roberts, I. Schmeltzer, H. Schulz, M. Siccha, M. Siddall, and G. Trommer (2008), New constraints on the timing of sea level fluctuations during early to middle marine isotope stage 3, *Paleoceanography*, *23*, PA3219, doi:10.1029/2008PA001617.
Romero, O., G. Mollenhauer, R. R. Schneider, and G. Wefer (2003), Oscillations of the siliceous imprint in the central Benguela Upwelling System from MIS 3 through to the early Holocene: The influence of the Southern Ocean, *J. Quat. Sci.*, *18*(8), 733–743.
Romero, O. E. (2010), Changes in style and intensity of production in the Southeastern Atlantic over the last 70,000 yr, *Mar. Micropaleontol.*, *74*(1–2), 15–28.
Romero, O. E., X. Crosta, J. H. Kim, L. Pichevin, and J. Crespin (2015), Rapid longitudinal migrations of the filament front off Namibia (SE Atlantic) during the past 70 kyr, *Global Planet. Change*, *125*, 1–12.
Sarmiento, J. L., N. Gruber, M. A. Brzezinski, and J. P. Dunne (2004), High-latitude controls of thermocline nutrients and low latitude biological productivity, *Nature*, *427*(6969), 56–60.
Sarnthein, M., G. Tetzlaff, B. Koopmann, K. Wolter, and U. Pflaumann (1981), Glacial and interglacial wind regimes over the eastern subtropical Atlantic and North-West Africa, *Nature*, *293*(17), 193–196.
Schmiedl, G., and A. Mackensen (1997), Late Quaternary paleoproductivity and deep water circulation in the eastern South Atlantic Ocean: Evidence from benthic foraminifera, *Palaeogeogr. Palaeoclimatol. Palaeoecol.*, *130*(1–4), 43–80.
Schneider, R. R., B. Price, P. J. Mueller, D. Kroon, and I. Alexander (1997), Monsoon related variations in Zaire (Congo) sediment load and influence of fluvial silicate supply on marine productivity in the east equatorial Atlantic during the last 200,000 years, *Paleoceanography*, *12*, 463–481.

Schukat, A., H. Auel, L. Teuber, N. Lahajnar, and W. Hagen (2014), Complex trophic interactions of calanoid copepods in the Benguela upwelling system, *J. Sea Res.*, *85*, 186–196.
Scussolini, P., G. Marino, G.-J. A. Brummer, and F. J. C. Peeters (2015), Saline Indian Ocean waters invaded the South Atlantic thermocline during glacial termination II, *Geology*, *43*, 139–142, doi:10.1130/G36238.1.
Shannon, L. V. (1985), The Benguela ecosystem: I. Evolution of the Benguela, physical features and processes, *Oceanogr. Mar. Biol.*, *23*, 105–182.
Shannon, L. V., and A. Jarre-Teichemann (1999), A model of trophic flows in the northern Benguela upwelling system during the 1980's, *South Afr. J. Mar. Sci.*, *21*, 349–366.
Shannon, L. V., and G. Nelson (1996), The Benguela: Large scale features and processes and system variability, in *The South Atlantic: Present and Past Circulation*, edited by G. Wefer et al., pp. 163–210, Springer, Berlin.
Shi, N., L. M. Dupont, H.-J. Beug, and R. Schneider (1998), Vegetation and climate changes during the last 21 kyrs in SW Africa based on a marine pollen record, *Veg. Hist. Archaeobotany*, *7*, 127–140.
Shi, N., L. M. Dupont, H.-J. Beug, and R. Schneider (2000), Correlation between vegetation in southwestern Africa and oceanic upwelling in the past 21,000 years, *Quat. Res.*, *54*(1), 72–80.
Shi, N., R. Schneider, H.-J. Beug, and L. M. Dupont (2001), Southeast trade wind variations during the last 125 kyr: Evidence from pollen spectra in eastern South Atlantic sediments, *Earth Planet. Sci. Lett.*, *187*, 311–321.
Shillington, F. A. (1998), *The Benguela Upwelling System off Southwestern Africa*, pp. 583–604, Harvard Univ. Press, Cambridge, USA.
Siddall, M., E. J. Rohling, A. Almogi-Labin, C. Hemleben, D. Meischner, I. Schmelzer, and D. A. Smeed (2003), Sea-level fluctuations during the last glacial cycle, *Nature*, *423*(6942), 853–858.
Siddall, M., E. J. Rohling, W. G. Thompson, and C. Waelbroeck (2008), Marine isotope stage 3 sea level fluctuations: Data synthesis and new outlook, *Rev. Geophys.*, *46*, RG4003, doi:10.1029/2007RG000226.
Stuut, J.-B. W., M. A. Prins, R. R. Schneider, G. J. Weltje, J. H. F. Jansen, and G. Postma (2002), A 300-kyr record of aridity and wind strength in southwestern Africa: Inferences from grain-size distributions of sediments on Walvis Ridge, SE Atlantic, *Mar. Geol.*, *180*(1–4), 221–233.
Stuut, J.-B. W., X. Crosta, K. Van der Borg, and R. R. Schneider (2004), The relationship between Antarctic sea ice and south-western African climate during the Late Quaternary, *Geology*, *32*(10), 909–912.
Summerhayes, C. P., D. Kroon, A. Rosell-Melé, R. W. Jordan, H. J. Schrader, R. Hearn, J. Villanueva, J. O. Grimalt, and G. Eglinton (1995), Variability in the Benguela Current upwelling system over the past 70,000 years, *Prog. Oceanogr.*, *35*(3), 207–251.
Sweetman, A. K., S. Sommer, O. Pfannkuche, and U. Witte (2009), Retarded response by macrofauna-size foraminifera to phytodetritus in a deep Norwegian fjord, *J. Foraminiferal Res.*, *39*(1), 15–22.
Sydeman, W. J., M. García-Reyes, D. S. Schoeman, R. R. Rykaczewski, S. A. Thompson, B. A. Black, and S. J. Bograd (2014), Climate change and wind intensification in coastal upwelling ecosystems, *Science*, *345*(6192), 77–80.
Toggweiler, J. R., J. L. Russell, and S. R. Carson (2006), Midlatitude westerlies, atmospheric CO_2, and climate change during the ice ages, *Paleoceanography*, *21*, PA2005, doi:10.1029/2005PA001154.
Tyson, P. D. (1986), *Climatic Change and Variability in Southern Africa*, 220 pp., Oxford Univ. Press, Cape Town.
Ufkes, E., J. H. F. Jansen, and R. R. Schneider (2000), Anomalous occurrences of *Neogloboquadrina pachyderma* (left) in a 420-ky upwelling record from Walvis Ridge (SE Atlantic), *Mar. Micropaleontol.*, *40*(1–2), 23–42.
Van der Zwaan, G. J., and F. J. Jorissen (1991), Biofacial patterns in river-induced shelf anoxia, in *Modern and Ancient Continental Shelf Anoxia*, *Spec. Publ.*, vol. 58, edited by R. V. Tyson and T. H. Pearson, pp. 65–82, Geological Society, London.
Van Leeuwen, R. J. W. (1989), Sea-floor distribution and Late Quaternary faunal patterns of planktonic and benthic foraminifera in the Angola Basin, *Utrecht Micropaleontol. Bull.*, *38*, 1–288.
Van Zinderen Bakker, E. M. (1967), Upper Pleistocene and Holocene stratigraphy and ecology on the basis of vegetation changes in sub-Saharan Africa, in *Background to Evolution in Africa*, edited by W. W. Bishop and J. D. Clark, pp. 125–147, Univ. of Chicago, Chicago.
Veres, D., et al. (2013), The Antarctic ice core chronology (AICC2012): An optimized multi-parameter and multi-site dating approach for the last 120 thousand years, *Clim. Past*, *9*(4), 1733–1748.
Waelbroeck, C., L. Labeyrie, E. Michel, J. C. Duplessy, J. F. McManus, K. Lambeck, E. Balbon, and M. Labracherie (2002), Sea-level and deep water temperature changes derived from benthic foraminifera isotopic records, *Quat. Sci. Rev.*, *21*(1–3), 295–305.
Weaver, A. J., O. A. Saenko, P. U. Clark, and J. X. Mitrovica (2003), Meltwater pulse 1A from Antarctica as a trigger of the Bølling-Allerød warm interval, *Science*, *299*(5613), 1709–1713.
Wefer, G., et. al. (1998), Proceedings of the Ocean Drilling Program Initial Reports, 1–577 pp., College Station, Tex.
Weltje, G. (1997), End-member modelling of compositional data: Numerical-statistical algorithms for solving the explicit mixing problem, *J. Math. Geol.*, *29*(4), 503–549.
Weltje, G. J., and M. A. Prins (2003), Muddled or mixed? Inferring palaeoclimate from size distributions of deep-sea clastics, *Sediment. Geol.*, *162*(1), 39–62.
WoRMS Editorial Board (2015), World Register of Marine Species. [Available at http://www.marinespecies.org at VLIZ. Accessed 2015-02-15.]